



1  
2  
3  
4  
5  
6  
7  
8  
9  
10  
11  
12  
13  
14  
15  
16  
17  
18  
19  
20  
21  
22  
23  
24  
25  
26  
27  
28  
29  
30  
31  
32  
33  
34  
35  
36  
37  
38  
39

## Measurement Report: Interpretation of Wide Range Particulate Matter Size Distributions in Delhi

Ülkü Alver Şahin<sup>1</sup>, Roy M Harrison<sup>2,a</sup>, Mohammed S. Alam<sup>2,b</sup>  
David C.S. Beddows<sup>2,3</sup>, Dimitrios Bousiotis<sup>2</sup>, Zongbo Shi<sup>2</sup>  
Leigh R. Crilley<sup>4</sup>, William Bloss<sup>2</sup>, James Brean<sup>2</sup>, Isha Khanna<sup>5,c</sup>  
and Rulan Verma<sup>6,c</sup>

<sup>1</sup> Istanbul University-Cerrahpaşa, Engineering Faculty Environmental  
Engineering Department, Istanbul, Turkey

<sup>2</sup> School of Geography, Earth and Environmental Sciences  
University of Birmingham, Birmingham, B15 2TT, UK

<sup>3</sup> National Centre for Atmospheric Science  
University of York, Heslington, York, YO10 5DQ, UK

<sup>4</sup> Department of Chemistry, York University  
Toronto, Ontario, M3J 1P3, Canada

<sup>5</sup> Puget Sound Clean Air Agency, Seattle, Washington, USA 98101

<sup>6</sup> Institute of research on catalysis and the environment of Lyon - IRCELYON  
Université De Lyon, 69626 Villeurbanne cedex, France

Corresponding author: E-mail: [r.m.harrison@bham.ac.uk](mailto:r.m.harrison@bham.ac.uk) (Roy M. Harrison)

<sup>a</sup> Also at: Department of Environmental Sciences / Centre of Excellence in Environmental  
Studies, King Abdulaziz University, PO Box 80203, Jeddah, 21589, Saudi Arabia

<sup>b</sup> Now at: School of Biosciences, University of Nottingham, Sutton Bonington  
Campus, Leicestershire, LE12 5RD

<sup>c</sup> Previously at: IIT Delhi, Hauz Khas, New Delhi, India 110016



40 **ABSTRACT**

41 Delhi is one of the world's most polluted cities, with very high concentrations of airborne  
42 particulate matter. However, little is known on the factors controlling the characteristics of particle  
43 number size distributions. Here, new measurements are reported from three field campaigns  
44 conducted in winter, pre-monsoon and post-monsoon seasons on the Indian Institute of Technology  
45 campus in the south of the city. Particle number size distributions were measured simultaneously  
46 using a Scanning Mobility Particle Sizer and a Grimm optical particle monitor, covering 15 nm to  
47  $>10\ \mu\text{m}$  diameter. The merged, wide-range size distributions were categorised into five size ranges:  
48 nucleation (15-20 nm), Aitken (20-100 nm), accumulation (100 nm-1  $\mu\text{m}$ ), large fine (1-2.5  $\mu\text{m}$ )  
49 and coarse (2.5-10  $\mu\text{m}$ ) particles. The ultrafine fraction (15-100 nm) accounts for about 52 % of all  
50 particles by number ( $\text{PN}_{10}$ ), but just 1 % by  $\text{PM}_{10}$  volume ( $\text{PV}_{10}$ ). The measured size distributions  
51 are markedly coarser than most from other parts of the world, but are consistent with earlier cascade  
52 impactor data from Delhi. Our results suggest substantial aerosol processing by coagulation,  
53 condensation and water uptake in the heavily polluted atmosphere, which takes place mostly at  
54 nighttime and in the morning hours. Total number concentrations are highest in winter, but the  
55 mode of the distribution is largest in the post-monsoon (autumn) season. The accumulation mode  
56 particles dominate the particle volume in autumn and winter, while the coarse mode dominates in  
57 summer. Polar plots show a huge variation between both size fractions in the same season and  
58 between seasons for the same size fraction. The diurnal pattern of particle numbers is strongly  
59 reflective of a road traffic influence upon concentrations, especially in autumn and winter. There is  
60 a clear influence of diesel traffic at nighttime when it is permitted to enter the city, and also  
61 indications in the size distribution data of a mode  $<15\ \text{nm}$ , probably attributable to CNG/LPG  
62 vehicles. New particle formation appears to be infrequent, and in this dataset is limited to one day  
63 in the summer campaign. Our results reveal that the very high emissions of airborne particles in  
64 Delhi, particularly from traffic, determine the variation of particle number size distributions.

65



66 **1. INTRODUCTION**

67 Air pollution in Delhi has been studied for many years, and the authorities have implemented several  
68 interventions designed to limit the concentrations. The sulphur content of diesel and petrol fuels was  
69 reduced to 50 ppm during 1996-2010, more than 1300 industries were shut down due to hazardous  
70 emissions, commercial vehicles older than 15 years were gradually taken out of the traffic fleet, and  
71 public transport vehicles and auto-rickshaws were converted to compressed natural gas (CNG) fuel  
72 (Narain and Krupnick, 2007). An odd–even vehicle number plate restriction has been applied during  
73 working days (Chowdhury et al., 2017). Although these measures have reduced gaseous pollutants  
74 (SO<sub>2</sub> and CO) and primary particulate matter, in recent years, several studies have reported that the  
75 PM<sub>2.5</sub> concentrations have been constant or slowly increasing in India, especially in the winter and  
76 autumn seasons (Babu et al., 2013; Balakrishnan et al., 2019; Dandona et al. 2017, Kumar et al.,  
77 2017), except in 2020. In 2020, the PM<sub>2.5</sub> level decreased by approximately 40 %, due to Covid-19  
78 measures (Rodríguez-Urrego and Rodríguez-Urrego 2020; Mahato et al., 2020). Although the overall  
79 emission sources in India are dominated by traffic, industry, construction, and local biomass burning,  
80 haze pollution events in Delhi are frequently related to the large-scale open burning of post-harvest  
81 crop residues/wood during the crop burning season in nearby rural regions (Cusworth et al. 2018;  
82 Bikkina et al. 2019; Kanawade et al., 2020). Although the sources of particles are mostly local (Hama  
83 et al., 2020), meteorological factors play an important role in influencing concentrations (Tiwari et  
84 al., 2014; Yadav et al., 2016; Guo et al., 2017; Dumka et al. 2019; Kumar et al. 2020).

85

86 Annual average PM<sub>2.5</sub> levels range between 81 and 190 µg/m<sup>3</sup> in Delhi and are clearly higher than  
87 the WHO guideline value (5 µg/m<sup>3</sup>) and Indian national limit value (40 µg/m<sup>3</sup>) (Hama et al., 2020).  
88 To the best of our knowledge, most studies in India have focussed on the source apportionment from  
89 chemical profiles of particles (Pant and Harrison, 2012; Jain et al. 2020; Bhandari et al., 2020; Rai  
90 et al., 2020). Mostly they have reported that biomass burning contributes greatly to PM<sub>2.5</sub> while traffic  
91 contributes heavily to PM<sub>10</sub> in Delhi. Residential energy use contributes 50 % of the PM<sub>2.5</sub>



92 concentration and the construction sectors are also evaluated as an important source of particles  
93 (Guttikunda et al., 2014; Butt et al., 2016; Conibear et al., 2018). Furthermore, it is particularly  
94 important to understand the absolute contribution and sources of different sizes of particles within  
95  $PM_{2.5}$ . A recently published paper by Das et al. (2021) highlighted that  $<250$  nm particles contribute  
96 a significant proportion of the total  $PM_{2.5}$  and are a potentially important link with human health.

97

98 The Particle Size Distribution (PSD) can provide air pollution source apportionment with high time  
99 resolution compared to use of chemical species, and influences the aerosol transport and  
100 transformation profiles in the urban atmosphere and toxicological effects on humans (Wu and Boor,  
101 2021). Many PSD studies have been conducted in urban, traffic and background sites over the past  
102 decades and three review studies have been published (Vu et al., 2015; Azimi et al., 2014; Wu and  
103 Boor, 2021). There are some studies evaluating the number or mass PSD in Delhi (Mönkkönen et al.,  
104 2005; Chelani et al., 2010; Gupta et al., 2011; Pant et al., 2016; Gani et al., 2020). Harrison (2020)  
105 compared PSDs from Delhi, Beijing and London and reported that the particles from Delhi are far  
106 greater in number with a much larger modal diameter, close to 100 nm. In a recent paper, Gani et al.  
107 (2020) has investigated the PSD up to  $0.5 \mu m$  sizes from 2017 to 2018 and reported that rapid  
108 coagulation is an important process in Delhi.

109

110 The wide range PSD is important to describe all sources of inhalable particles ( $<10 \mu m$ ). It is not easy  
111 to separate particles arising from resuspension, sea salt and construction, or from brake wear and  
112 combustion or vehicle exhaust, using only  $<0.5 \mu m$  particle sizes. Harrison et al. 2011 reported that  
113 using wide range particle sizes in source apportionment is extremely successful in identifying the  
114 separate contributions of on-road emission including brake wear and resuspension. Although there  
115 are a few studies of wide range particle characterization in Beijing (Jing et al., 2014) and source  
116 apportionment in Venice, Italy (Masiol et al., 2016), there has been no wide range PSD study in Delhi.  
117 In this study, we aimed to interpret particulate matter size distributions over a wide range (15 nm to



118 10  $\mu\text{m}$ ) in the winter, post-monsoon and pre-monsoon seasons in Delhi. Future studies will look at  
119 two-step receptor modelling of wide range particulate matter size distributions and chemical  
120 composition in Delhi.

121

## 122 2. METHODS

### 123 2.1 Study Area

124 The measurements were part of the NERC/MoES Air Pollution and Human Health in an Indian mega-  
125 city (APHH-Delhi, [www.urbanair-india.org](http://www.urbanair-india.org)) study, a joint UK-India project addressing air pollution  
126 in Delhi. The sampling location was  $\sim 15$  m above ground level on the 4<sup>th</sup> floor of the Civil  
127 Engineering Department at the Indian Institute of Technology Delhi (IIT Delhi) campus, located in  
128 New Delhi, representative of an urban background environment (28.545 N, 77.193 E) (Figure S1).  
129 As part of APHH-Delhi, there were three field campaigns: (i) Jan-Feb 2018 (winter), (ii) May-June  
130 2018 (summer; pre-monsoon) and (iii) Oct-Nov 2018 (autumn; post-monsoon). In all field  
131 campaigns, a suite of gas and particulate phase instrumentation was deployed within a temperature  
132 controlled laboratory.

133

134 These sampling periods were representative of conditions for PM and gases during these seasons in  
135 Delhi. We found the average  $\text{PM}_{2.5}$  concentration to be approximately  $180 \mu\text{g}/\text{m}^3$ ,  $220 \mu\text{g}/\text{m}^3$  and  $120$   
136  $\mu\text{g}/\text{m}^3$  for winter, autumn (excluding Diwali) and summer, respectively measured by a TEOM-  
137 FDMS. Hama et al. (2020) studied the long term (from 2014 to 2017) trends of air pollution in Delhi  
138 at 6 stations (residential, commercial, and industrial sites) and reported that the mean  $\text{PM}_{2.5}$   
139 concentrations ranged between  $147 - 248 \mu\text{g}/\text{m}^3$ ,  $147 - 248 \mu\text{g}/\text{m}^3$  and  $76 - 135 \mu\text{g}/\text{m}^3$  for winter,  
140 autumn and summer, respectively, and a good correlation between sites within Delhi. This gives  
141 reassurance that the  $\text{PM}_{2.5}$  concentrations measured at our site are within the typical range of those  
142 observed in Delhi.

143



144 **2.2 Measurements**

145 To measure the particle size range used in this study, two particle instruments were used to collect  
146 number size distributions (NSD). For the range 15-640nm, a TSI SMPS 3936 was used, consisting  
147 of a TSI 3080 Electrostatic Classifier, TSI 3081 DMA and TSI 3775 CPC. To extend this range into  
148 the coarse mode a GRIMM 1.108 Portable Laser Aerosol Spectrometer and Dust Monitor were used  
149 alongside the SMPS.

150

151 Aerosol particle sizes in the atmosphere span a very wide range from a few nanometers at the lower  
152 end to some tens of micrometers at the upper end. Because of this very wide range of sizes, particle  
153 properties vary considerably across the size spectrum with the behaviour of the smaller particles being  
154 determined by their high mobility and hence diffusivity, whilst at the coarse end of the size  
155 distribution inertial properties are especially important. Due to this divergence in behaviour, no  
156 instrument is capable of measurement of the whole range of particle sizes. The smaller particles are  
157 mostly measured as a function of their electric mobility when charged, while the larger particles are  
158 counted using their inertial or optical properties. In this study an SMPS (Scanning mobility particle  
159 sizer) based on mobility diameters and a GRIMM optical spectrometer were used to count smaller  
160 and larger particles, respectively.

161

162 **2.3 Merging Process**

163 Merging procedures have usually been reported for merging SMPS and APS (Aerosol Particle Sizer)  
164 data, but here GRIMM data is merged with SMPS data. For a complete particle size distribution,  
165 paired hourly averaged particle number size distributions collected from the SMPS and GRIMM were  
166 merged. The merging procedure is based on the principle of converting the diameters of the GRIMM-  
167 derived data to a diameter matching the SMPS-derived data, in the region where the size distribution  
168 measurements overlap. The GRIMM measures the optical diameter  $d_b^t$  whereas the SMPS measures  
169 the mobility diameter  $d_a^t$  of the particles. Comprehensive descriptions of the procedure and



170 mathematics are given by DeCarlo et al. (2004) and Schmid et al. (2007). The GRIMM NSD are  
171 translated onto the extended electrical mobility diameter axis of the SMPS using equation (R1)  
172 (Beddows et al. 2010; Liu et al., 2016; Ondracek et al., 2009).

173

$$174 \quad d_b^t = \frac{d_a^t}{X} \sqrt{\frac{C(d_a^t)}{C(d_b^t)}} \quad (R1)$$

175

176 The Cunningham slip correction factor is given by  $C$  and the unknown variables such as the shape  
177 factor of the particles are accounted for by a free parameter  $X$  (given by equation R2) which is adjusted  
178 until the tails of the SMPS and GRIMM NSD overlap each other giving a continuous NSD across the  
179 particle size bins measured by the two instruments.

180

$$181 \quad X = \sqrt{\frac{\rho_e^t}{\rho_o}} \quad (R2)$$

182

183 The estimated transition-regime effective density  $\rho_e^t$  (normalised by the unit density,  $\rho_o$ ) typically  
184 ranges from 0.77 to 2.56 g/cm<sup>3</sup> when aerodynamic diameter is used in merging. Detailed  
185 information upon the effective particle density based on the geographical regions is seen in the Wu  
186 and Boor (2021) study.

187

188 The merging algorithm (originally programmed in CRAN R) was implemented using Excel  
189 spreadsheets and the solver tool minimised the separation between the tails of the overlapping SMPS  
190 and GRIMM. Due to the imperfect nature of the data, each of the merges was allocated a factor  
191 indicating quality based on whether: (i) there is a successful fit; (ii) the scatter of the data across the  
192 overlapping tails; (iii) the fraction of points on the tail falling onto the fitted curve; and (iv) how  
193 smooth the overlap is (Table S1). The size bins overlap (300-700 nm) between Grimm and SMPS.  
194 This process was repeated for the winter, summer and autumn data sets and any results failing the test



195 were either repeated or the data removed from the analysis. In all, only 8 samples from 1117 failed  
196 to give an acceptable fit in the merge procedure.

197

#### 198 **2.4 Data and Quality Management**

199 Data from SMPS and GRIMM were measured with 1-min resolution. In this study, data sets were  
200 used by taking their hourly averages. Simultaneous measurement data from the SMPS and GRIMM  
201 were used. The seasons were categorized as winter, autumn and summer. The measurements were  
202 taken in winter from 12 January 16:00 to 11 February 04:00, in autumn from 24 October 16:00 to 11  
203 November 10:00, in summer 16 May 19:00 to 05 June 15:00 in 2018. There were 709, 403 and 477  
204 total pairs (hours) in the data sets in winter, autumn and summer, respectively. But 172, 43 and 257  
205 pairs in winter, autumn and summer, respectively were excluded because of the non-availability of  
206 data at that time. Data coverage is 76 % for winter, 95 % for autumn and 46 % for summer. Figure  
207 S2 in the Supplementary shows hourly mean values of total particle counts for three seasons. In order  
208 to evaluate day and night time PNC (particle number concentration) differences, the day and night  
209 were defined as 07:00-19:00 and 19:00 – 07:00, respectively. All times reported are local times  
210 recorded in Indian Standard Time (IST; GMT+05:30).

211

212 R version 3.1.2 was used to analyse the data (R Core Team, 2015). Firstly, all data were checked for  
213 clean-up of the robustness of the data sets, to detect anomalous records and take out the extreme  
214 values. Data greater than the 99.5<sup>th</sup> percentile were deleted. Diwali time in 2018 (7<sup>th</sup> of November  
215 2018 from 16:00 to 23:00) was taken out the data set in order to exclude its extreme effect on PSD  
216 values. Particle number concentrations during Diwali time are given in the Supplementary, Figure  
217 S3. There were some single gaps in the data matrixes. These missing data were replaced by linearly  
218 interpolated values from the nearest bins to those samples.

219



220 In the literature, PNCs measured below 1  $\mu\text{m}$  are frequently split into three ranges: nucleation, Aitken  
221 and accumulation (Gani et al., 2020). Size range of modes can be highly variable according to the  
222 description of the nucleation size range and maximum measured size. Nucleation size ranges have  
223 been described as below 30 nm (Masiol et al. 2016) or below 25 nm (Gani et al., 2020) or below 20  
224 nm (Wu and Boor, 2021). Despite this, there are also limited studies on wide range PSD, some  
225 evaluating wide range PSDs split into 4 ranges (nucleation, Aitken, accumulation and coarse) (Masiol  
226 et al. 2016; Harrison et al., 2011). In this study, the modes have been aggregated into five size groups:  
227 nucleation (15-20 nm), Aitken (20 -100 nm), accumulation (100 nm – 1  $\mu\text{m}$ ), large fine (1  $\mu\text{m}$  – 2.5  
228  $\mu\text{m}$ ) and coarse (2.5  $\mu\text{m}$  – 10  $\mu\text{m}$ ) based on merged data using SMPS and GRIMM observations.  
229 Ultrafine particles (UFP) are considered to be total PN counts of Nucleation and Aitken modes (<100  
230 nm).

231

232 The particle mass was calculated for the SMPS+Grimm merged data, assuming a density of 1.6 g  $\text{cm}^{-3}$   
233 (Gani et al., 2020). Figure S4 shows the comparison of  $\text{PM}_{2.5}$  measured by SMPS+GRIMM and  
234 TEOM-FDMS in Delhi for the three seasons. Figure S5 shows the comparison of  $\text{PM}_{2.5}$  with relative  
235 humidity measured by SMPS+GRIMM and TEOM in Delhi for the three seasons. A good correlation  
236 of the estimated particle mass with independent measurements with a co-located TEOM-FDMS was  
237 observed, except in summer.

238

### 239 3. RESULTS

#### 240 3.1 Particle Number and Size

241 Table S2 gives the descriptive statistics of particle number counts ( $\#/\text{cm}^3$ ) calculated using every 1-  
242 hour measurements for the nucleation, Aitken, accumulation, large fine and coarse modes between  
243 15 nm and 10  $\mu\text{m}$  in all seasons. Time series of total particle number counts are presented in Figure  
244 S2. The average total PN levels were 36,730  $\#/\text{cm}^3$  in winter, 29,355  $\#/\text{cm}^3$  in autumn and 18,906  
245  $\#/\text{cm}^3$  in summer. Generally, the wintertime PN levels were higher than the other seasons. The



246 wintertime PN levels of nucleation, Aitken and accumulation modes were  $\sim 1.5$ , 1.8 and 2.2 times  
247 higher than in summer, respectively. Similar ratios were obtained by Guttikunda and Gurjar (2012)  
248 in Delhi for particulate matter concentrations. This is attributed to the unfavorable dispersion  
249 conditions, including low wind speed and low mixing height during the winter season. The autumn  
250 PN levels of nucleation, Aitken and accumulation modes were  $\sim 1.5$ , 1.3 and 1.9 times higher than in  
251 summer, respectively. The wintertime and autumn average PN levels are similar except for the Aitken  
252 mode for which winter is 1.4 times higher than in autumn. However, for the large fine and coarse  
253 modes the PN level was not markedly different between winter, autumn, and summer. Gani et al.  
254 (2020) reported that the average PN levels were 52,500  $\#/cm^3$  in winter, 43,400 in summer, and  
255 38,000  $\#/cm^3$  in autumn in Delhi measured in 2017. The differences in the magnitude of number  
256 counts between the two studies are potentially explained by the difference in the sampling time and  
257 changes in emissions.

258

259 Figure 1 shows a comparison of average particle number and volume and the contribution to total  
260 PN. The average PV (particle volume) levels indicate that PV of the Aitken mode is highest in winter,  
261 while the accumulation mode is highest in autumn and the coarse mode is highest in summer. The  
262 contribution of UFP( $<100nm$ ) to numbers is highest in summer (57 %) but their contribution to  
263 volume is the lowest in autumn and summer ( $<1$  %). The contribution to both number and volume  
264 of the accumulation mode is highest in autumn with 51 % and 75 %, respectively. UFP contributions  
265 to total PV are below 1 % in Delhi. Furthermore, it can be seen clearly that the coarse fraction of  
266 particles dominates in summer, while the accumulation mode dominates in autumn and winter.

267 Wu and Boor (2021) analysed the PSD observations made between 1998 and 2017 in 114 cities in 43  
268 countries around the globe. They reported that there are significant variations in the magnitude of  
269 urban aerosol PSD among different geographical regions. The main finding of their study is that the  
270 number PSD in Europe, North America, Australia, and New Zealand are dominated by nucleation-  
271 and Aitken-mode particles while in Central, South, Southeast and East Asia they are dominated by



272 the substantial contribution from the accumulation mode, which is consistent with our finding. Pant  
273 et al. (2016) report mass size distributions for particulate matter sampled by cascade impactor in Delhi  
274 in winter. The dominant modes appear at around 3-4  $\mu\text{m}$  and 0.6  $\mu\text{m}$ , with a lesser peak at 0.2  $\mu\text{m}$   
275 aerodynamic diameter. These are respectively in the coarse (former mode) and accumulation (latter  
276 two modes) ranges as classified in the current study. The largest component of mass was in the  
277 accumulation mode, and the distribution fits well with the pattern of data seen in Figure 1. Major  
278 components of the coarse fraction were Al, Si, Ca and Fe (Pant et al., 2016), suggestive of soil and  
279 street dust as major contributors. The elements most notably in the accumulation fraction were Cu,  
280 Zn, Pb and Sb, indicative of non-exhaust traffic emissions and metallurgical sources, and S, which  
281 showed a major peak due to sulphate, peaking at 0.9  $\mu\text{m}$  (Pant et al., 2016).

282

283

### 284 3.2 Diurnal Change

285 Figure 2 shows the diurnal variation of particle number concentrations and of  $\text{PM}_{2.5}$ , BC, NO and  
286  $\text{NO}_2$  for each season (excluding the day of Diwali), and the normalized time variations of all particle  
287 fractions are given in Figure S6. Figure S7 represents the diurnal variation of meteorological  
288 parameters. In general, there are large differences of PN levels between cold seasons (winter and  
289 autumn) and warm season (summer) for nucleation size particles. Coarse mode particle numbers in  
290 the summer are higher than in winter and autumn, except in the evening time. For autumn and winter,  
291 particle counts are similar from 7 am to 7 pm (daytime). However, from 7 pm to 7 am particle counts  
292 in winter are higher than in autumn. The lowest levels for all modes were present during the afternoon  
293 in all seasons (2-4 pm), followed by highest levels during the night in winter (after 8 pm). The winter  
294 and autumn diurnal profiles had two peaks for below 1  $\mu\text{m}$  particle size in the morning and evening  
295 corresponding to the traffic rush hours. But in the summer the same peaks for nucleation, Aitken and  
296 accumulation modes are seen although of smaller magnitude, and one hour earlier comparing to the  
297 winter and autumn. Pant et al. (2016) reported the diurnal variation of traffic at one of the major  
298 arterial roads in Delhi and Dhyani et al. (2019) reported on traffic-related emission. Figure S8 shows



299 the diurnal variation in traffic at a major road intersection in Delhi. Cars, two/three wheelers, bus and  
300 LCV (light commercial vehicle) fleet numbers increase in the morning, persist throughout daytime  
301 and start to decrease at 22:00. Due to the prohibition of access for heavy-duty diesel vehicles to central  
302 Delhi from 6:00 am until 11:00 pm in the night, during the daytime including the traffic rush hours  
303 the HCV (heavy commercial vehicles) number is at its lowest level (Figure S8 or Dhyani et al. 2019).  
304 Small midday PN peaks were observed during the summer in the nucleation, Aitken and coarse  
305 modes. Another study conducted in Delhi reported the same midday peaks in the warm season and  
306 the highest levels in the cold season (Gani et al. 2020), which may be related to bus and LCV  
307 emissions at midday.

308

309 Figure 3 shows the differences in diurnal variations of total PN levels between the weekday and  
310 weekend. These are based upon a small dataset, and hence the rather small differences within a season  
311 may not be meaningful. In winter the PN levels on Saturday and Sunday are higher than on the  
312 weekdays during the night (from 8 pm to 10 am the next day). However, after the morning rush hour  
313 peaks, during the daytime the PN levels are the same for all days. The diurnal variation of PN in the  
314 autumn shows no significant differences among the days with the same main peaks in the morning  
315 for all days, although highest on Saturday. There is a flattened peak (from 8 to 10 am) in the morning  
316 rush hour for the weekday while there are pointed peaks at approximately 9 am on Saturday and  
317 Sunday in winter and autumn. Measurements made during the summer period are very limited. Due  
318 to there being only 4 full days and 9 half days of measurements, it is very hard to draw any  
319 conclusions. Even so, there are indications of a weekday traffic effect upon the PN levels in summer.  
320 There is only one day of measurements on a Sunday (3<sup>rd</sup> June 2018) and it shows the midday peaks.  
321 Overall, despite seasonal differences, there appears to be a strong influence of light duty road vehicles  
322 upon the diurnal profiles, reflecting traffic volumes, with an impact of heavy duty vehicles upon  
323 nighttime concentrations of all particle fractions.

324



325 NPF events present variable seasonality for different areas, though in most cases they appear to be  
326 more frequent during spring or summer (Salvador et al., 2021). Gani et al. 2020 studied long term  
327 PSD in Delhi and have stated that they did not see any NPF during the winter or autumn seasons in  
328 Delhi. In this study, the identification of NPF events was conducted manually using the criteria set  
329 by Dal Maso et al. (2005) and used by Bousiotis et al (2019; 2021). The data were analysed visually  
330 on a day-to-day basis: each 24-hour period, from midnight to midnight. According to these criteria, a  
331 NPF event is considered when: a distinctly new mode of particles appears in the nucleation mode size  
332 range, prevails for some hours, and shows signs of growth. These are the initial criteria used in  
333 identifying the events. Following that, as the dataset starts from a rather large size (15 nm), to be  
334 more confident about the events and not to confuse them with pollution events, high time resolution  
335 data for NO<sub>x</sub> as well as the fluctuations of the condensation sink were also used to identify pollution  
336 events affecting particle concentrations which were not considered. Hence, while we checked the  
337 particle size distributions for the NPF events, we also looked at the levels of pollutants to ensure that  
338 what was attributed to a NPF event was not particles from pollution / direct emissions. By considering  
339 the pollution levels and condensation sink we can reduce the possibility of including particle  
340 formation events that are not associated with secondary formation. After analysing all data,  
341 measurements from only one day during the measurement campaign were compliant with the criteria  
342 set as a class Ia NPF event. Figure 4 presents the contour plots of average diurnal variation for all  
343 seasons and for the NPF event on 3rd June. NPF may be suppressed due to very high pre-existing  
344 aerosol concentrations (Kanawade et al., 2020; Gani et al. 2020) during severe air pollution episodes  
345 in Delhi. This suppression effect has also been observed in European cities (Bousiotis et al., 2019;  
346 2021).

347

### 348 **3.3 Day and Night Time Differences in PN and PV**

349 Table S3 presents the summary statistics of the particle number and mass levels derived from merged  
350 particle number data and BC, NO<sub>x</sub> and PM<sub>2.5</sub> at night and day for each season, excluding Diwali.  
351 Figure 5 shows the particle number comparison of all modes at night and day seasonally. In both



352 night and day, the nucleation counts are approximately the same in autumn and summer ( $N/D=1.1$   
353 and 1.0), and a little higher at night in winter ( $N/D=1.3$ ). But in the night, Aitken and accumulation  
354 counts are higher than in the day by factors of 1.4 and 1.5 times in summer, 1.2 and 1.5 times in  
355 autumn, respectively and approximately 2 in winter. While the coarse mode PN counts are  
356 approximately the same for all seasons and day / night, the large fine PN level in the nighttime are  
357 significantly higher (1.7) than in the daytime in summer. It seems that in the nighttime high PM  
358 concentrations are due to the increasing Aitken and accumulation modes occurring from coagulation  
359 of nucleation mode particles, condensation of low volatility species or hygroscopic growth. In  
360 addition, biomass burning and older diesel vehicles can contribute significantly to particles in these  
361 fractions (Kumar et al., 2013; Chen et al., 2017; Gani et al., 2020). Meteorological factors can also  
362 profoundly affect the PN levels in daytime and nighttime. The differences of wind speed between day  
363 and night in summer are lower than in winter and autumn (Figure S7). Higher wind speed, and lower  
364 humidity, may favour the resuspension of coarse dust as a dominant mechanism in the summer.  
365 Seasonal changes in mixing depths are surprisingly small (Figure S7) and hence unlikely to have a  
366 major influence.

367

368 Overall, for the daytime for all seasons, hourly averaged UFP ( $<100\text{nm}$ ) concentrations are usually  
369 less than the nighttime, however the UFP contribution to the  $PN_1$  (55 % in day, 50 % in night for  
370 winter; 52 % in day, 45 % in night for autumn; 58 % in day, 56 % in night for summer) and  $PN_{10}$  (38  
371 % in day, 38 % in night for winter; 40 % in day, 33 % in night for autumn; 36 % in day, 33 % in night  
372 for summer) are mostly slightly higher in the daytime. Similarly, Gani et al. (2020) have reported the  
373 highest contribution (of UFP to PNC) in the daytime compared with the nighttime in Delhi. Due to  
374 the difference of PN size range (they measured down to 12nm), they found the UFP contribution to  
375 PNC higher than in the present study.

376

377

378



### 379 **3.4 Size Distributions**

380 Figure 5 shows the average particle number size distributions in three seasons in Delhi. Volume and  
381 Area distributions are shown in the Supplementary Materials in Figure S9. The highest number  
382 concentrations are seen in winter, followed by autumn, and then summer. Although the number  
383 concentrations of particles below 200 nm are far greater in winter those between 200 and 600nm are  
384 greater in autumn, within the accumulation mode. The winter and summer PSD show modes at  
385 approximately 100 nm but the autumn PSD shows the mode at approximately 200 nm. This could be  
386 due to changing sources of particles in Delhi between seasons (Jain et al. 2020), in addition to  
387 (differing) aerosol dynamical processes. The Delhi atmosphere is more polluted comparing with most  
388 other cities based on particle number and mass (Harrison, 2020). This will cause a tendency for  
389 particles to grow more rapidly by coagulation and condensation (Harrison et al., 2018), but this might  
390 be expected to occur in all seasons.

391

392 As described above, in Delhi the nighttime particle concentrations are markedly higher than the  
393 daytime concentrations. The PSD changes for each hour of the day across all three seasons were  
394 analysed (Figure S10) and categorized. Figure 7 presents the PSD differences between daytime and  
395 nighttime and shows the variation in PSDs within the day in all seasons. The main difference between  
396 day and night in winter is only the number concentration, with little change in the mode size between  
397 day and night, while the PSDs in summer and autumn show bimodal distributions with modes at  
398 approximately 30 and 140 nm in summer, and 35 and 200 nm in autumn. When we focus on PSD  
399 during the daytime, it can be clearly seen that the modes are manifest at different times: In winter,  
400 while the PSD shows the same mode at approximately 100 nm from 8 am to 2 pm, the mode in the  
401 afternoon (from 2 pm to 6 pm) drops slightly in size (70 nm). In the morning and afternoon there are  
402 two small peaks at 60 nm and 40 nm for the Aitken fraction and 170 and 130 nm for the accumulation  
403 fraction in autumn. During the day in summer, there are two peaks at approximately 30 nm from 10  
404 am to 6 pm. This may be associated with summer nucleation events and NPF on 3rd June 2018 (Figure



405 4). Furthermore it may be related to the growth of particles from 10 am to 2 pm in autumn and  
406 summer. The full reasons for these changing PSDs are not clear, and it would be unwise to attempt a  
407 detailed interpretation of a very small dataset.

408

409 Figure 8 shows the average geometric mean diameter (GMD) change with hour of the day. Two  
410 overall periods of GMD increase are observed. One of them is in nighttime in all seasons with GMD  
411 growing at between 4.6 nm/hour in summer and 6.2 nm/hour in winter. The particle growth in autumn  
412 is predominantly (when compared to the winter and summer) both late in the night (from 0 am to 5  
413 am) and in the morning (from 8 am to 12 pm). Considering the PSD trend in autumn (Figure 7), the  
414 GMD rises at 9 nm/hour from morning to noon. Similar results were obtained in the USA (Kuang et  
415 al., 2012), Canada (Jeong et al., 2010; Iida et al. 2008), Italy (Hamed et al., 2007) and Japan (Han et  
416 al. 2013). However the calculated GMD growth rate is smaller than that calculated by Sarangi et al.,  
417 (2015; 2018) in Delhi, by Kalafut-Pettibone et al. (2011) in Mexico City and by Zhang et al. (2011)  
418 in Beijing. The changing GMD with time in Delhi could be the result of changing sources, and/or of  
419 dynamics. Nocturnal growth may be the result of reducing temperatures and increasing RH causing  
420 vapour condensation (Sarangi et al., 2018). Morning growth may be due to oxidation processes  
421 leading to production of less volatile vapours which then condense onto the particles (Sarangi et al.  
422 2018).

423

424 Figure 9 gives the average particle number, volume, area and mass size distribution for all seasons.  
425 While the number size distributions have one mode, two peaks are observed in volume distributions,  
426 centered at 0.5  $\mu\text{m}$  and 6  $\mu\text{m}$ . These relate to two different main sources, which might be secondary  
427 aerosol (such as sulphate at high RH) in the fine mode and road dust resuspension, soil or construction  
428 dust for the coarse mode (Pant et al. 2016). In winter and autumn fine mode particle volumes are  
429 higher than the coarse mode. However, in summer the coarse mode particle volumes are higher than  
430 the fine particle level. In a recent paper, Thamban et al. (2021) show that modes in the mass size



431 distributions of HOA, SVOOA, BBOA and LVOOA measured by aerosol mass spectrometry are  
432 typically in the range 300-600nm vacuum aerodynamic diameter, very consistent with the peaks seen  
433 in the mass distributions in Figure 9.

434

435 Hama et al. (2020) obtained the spatiotemporal characteristics of daily-averaged air pollutants and  
436 concluded that the particulate matter mass ( $PM_{10}$  and  $PM_{2.5}$ ) is dominated by local sources across  
437 Delhi. The main local air pollutant sources in Delhi include traffic, construction, resuspension of dust,  
438 diesel generators, power plants, industries and biomass burning (Kumar et al., 2013; Nagpure et al.,  
439 2015; Hama et al., 2020).

440

441 All average PSD graphs show an increasing trend in PNC at particle sizes below 19 nm particle  
442 diameter. SMPS measurements in this study were conducted only above 15 nm. So, the peak particle  
443 size within this size range cannot be seen. However, the clear increase in particle number below 19  
444 nm indicates that another source may be important in Delhi. This small mode and bimodal PSD during  
445 the day (Figure 7) may be associated with the road transport vehicle types in Delhi. Despite the diesel  
446 restriction during the rush hours and conversion of the public transport vehicles to CNG, several  
447 studies have reported that  $PM_{2.5}$  concentrations have been remaining steady or are slowly increasing  
448 in India, especially in the winter and autumn seasons (Babu et al., 2013; Balakrishnan et al., 2019;  
449 Dandona et al. 2017; Kumar et al., 2017).

450

451 The fuels used in Delhi's traffic fleet are petrol, diesel, CNG and LPG. Legislation limits the sulphur  
452 content of the fuel to 50 ppm in diesel as per Bharat Stage IV. The diesel vehicles are not required to  
453 be fitted with particle traps. The technology of the gasoline vehicle fleet varies as vehicle engine  
454 capacity changes. Cars, two/three wheelers, bus and LCV fleet volumes are high during the day. Due  
455 to the time restrictions on trucks/heavy good vehicles entering the city, during the daytime the HCV  
456 number is at its lowest level (Figure S8).



457 Previous published studies indicate that emissions of particles from CNG vehicles (Euro 4, 5, 6) with  
458 diameter greater than 23 nm are as low as a diesel particle filter equipped vehicle, and an order of  
459 magnitude lower than gasoline vehicles (Kontses et al. 2020; Giechaskiel, et al. 2019; Magara-Gomez  
460 et al. 2014; Schreiber et al. 2007), and CNG vehicles mainly emit nuclei-mode particles (Zhu et a.,  
461 2014; Toumasatos et al. (2020). Zhu et al. (2014) calculated size-resolved particle emission factors  
462 from on-road diesel buses and CNG buses and reported that the PSD of diesel buses dominate the  
463 accumulation mode diameters of 74-87 nm while the PSD of CNG buses dominated the nucleation  
464 mode with modes at 21-24 nm. Total PN emissions of diesel buses per vehicle were 4 times higher  
465 than the level of CNG buses. However, the PN level in the nucleation mode (15-25 nm) of CNG buses  
466 was 1.7 times higher than from the diesel buses in the nucleation mode. Toumasatos et al. (2020)  
467 studied the particle emission performance of the Euro 6 CNG and gasoline vehicles and discussed the  
468 current EU cut-off solid PN size threshold of 23 nm. The results revealed that  $PN > 23$  nm represented  
469 43 % of  $PN > 10$  nm and 8 % of  $PN > 2.5$  nm for gasoline vehicles and 7 % of  $PN > 10$  nm and 1 % of  
470  $PN > 2.5$  nm for CNG vehicles respectively. These studies of emission PSDs show that a significant  
471 number of particles reside below the EU lower measurement limit of of 23 nm, and many are even  
472 smaller than 10 nm. These probably contribute to the mode seen just appearing at the extreme small  
473 particle limit of Figure 9.

474

475 When the PSD results measured in Delhi are compared with the main emission categories in the  
476 literature (Kumar et al., 2013; Vu et al., 2015), it seems that the average size distributions measured  
477 in the atmosphere in Delhi are much coarser, which is presumably due to condensation and  
478 coagulation, or it could be that secondary particles dominate over the primary emissions. Pant et al.  
479 (2016) hypothesised that the main accumulation mode peak in their winter measurements arose from  
480 aqueous droplet evaporation, although this mechanism would be unlikely to explain the mode seen  
481 in the summer data. Thamban et al. (2021) have also reported particle growth in the Delhi atmosphere  
482 from condensation of organic compounds formed from oxidation processes.



483 Previous studies have attempted to quantify the relative contribution of primary and secondary  
484 sources to the total and mode-segregated particle number concentrations (Kulmala et al. 2021;  
485 Casquero-Vera et al. 2021; Hama et al. 2017; Kulmala et al. 2016; Rodríguez, & Cuevas, 2007).  
486 Rodríguez and Cuevas (2007) first presented the methodology for the separation of traffic related  
487 primary aerosol particles from the total using the BC as the main tracer of traffic. The method was  
488 tested in this study, but did not prove appropriate as the BC sources in Delhi are more complex, and  
489 arise not only from traffic. The BC diurnal trend (Figure 2) does not show the rush hour peaks, and  
490 reflects mostly the combustion activity at night, presumably including the heavy duty diesel  
491 emissions. A recent study by Kulmala et al. (2021) used NO<sub>x</sub> as a tracer of primary sources. Figure 2  
492 shows that only the NO<sub>2</sub> diurnal trend in autumn is clearly related to traffic sources. Furthermore the  
493 sources of BC and NO<sub>x</sub> are largely the same, as judged from the high similarity between BC and NO<sub>x</sub>  
494 diurnal trends (Figure 2).

495

### 496 **3.5 Correlations of PN with NO<sub>2</sub>, NO, and BC**

497 Figure 10 shows the correlation coefficients between the hourly average PNs of five particle size  
498 fractions and NO, NO<sub>2</sub>, and BC measured in Delhi. Nucleation mode PN is better correlated with the  
499 Aitken mode PN in winter and summer despite the lower correlation in autumn. The correlations  
500 among >1 μm size fractions are higher in summer than winter and autumn. Tyagi et al. (2016) stated  
501 that the major source of NO<sub>x</sub> emissions is vehicle exhaust and power plants in Delhi. Furthermore,  
502 studies have reported that approximately 80-90 % of NO<sub>x</sub> and CO are produced from the transport  
503 sector in Delhi (Gurjar et al., 2004; Gulia et al., 2015; Tyagi et al., 2016; Hama et al., 2020). As seen  
504 in Figure 2, the NO<sub>2</sub> diurnal trend is very similar to nucleation and Aitken particle trends, especially  
505 in the autumn. NO<sub>2</sub> peaks in autumn in the traffic rush hours are larger than in winter and summer.  
506 In addition, there are no significant correlations between NO<sub>2</sub> and NO or BC in autumn (0.02 for NO,  
507 0.03 for BC) compared to the summer (0.73 for NO, 0.61 for BC) and winter (0.37 for NO and 0.28  
508 for BC) (Figure S11). NO and BC diurnal trends show the same higher level in the night (Figure 2)



509 and also, they have higher correlation coefficients (0.78 in winter, 0.77 in summer, 0.72 in autumn)  
510 for all seasons, similar to the accumulation mode particle counts (Figure 2, Figure 10, Table S2). NO<sub>2</sub>  
511 and <100 nm particles may be associated with traffic sources, while the NO and BC and <1 μm  
512 particles could be associated with biomass burning, industry, (small generator) power generation, or  
513 possibly also with diesel vehicles.

514

### 515 **3.6 Wind Effects**

516 Figure S12 represents polar plots of BC, NO and NO<sub>2</sub> measured in Delhi. This shows no consistent  
517 pattern. There are differences between the pollutants in terms of directional and wind speed  
518 associations, and for each pollutant / season. There is no obvious indication of a strong local source  
519 influence, typically manifest as an intense area in the very centre of the plot circle. The plots for the  
520 particle size fractions (Figure 11) also show little consistency between seasons for a given size  
521 fraction. Within a season, however, adjacent size fractions often show a similarity of behaviour  
522 (consistent with their correlations, see above) but this similarity does not extend across all size ranges  
523 within a season.

524

## 525 **4. CONCLUSIONS**

526 This study serves to highlight the remarkable complexity of airborne particulate matter in Delhi. The  
527 size distributions show marked seasonal changes, with coarse particles dominant in summer, but not  
528 in the cooler seasons, when the accumulation mode dominates. The measured size distributions show  
529 a fine mode aerosol with a considerably larger modal diameter than that typically seen in western  
530 countries, and larger than the modal emission size from major source categories. It appears that  
531 the high particle concentrations and chemically reactive atmosphere are promoting rapid coagulation  
532 and condensational growth of particles, and therefore the measured size distributions are driven more  
533 by aerosol dynamical processes than source characteristics. Growth via a liquid droplet phase in the  
534 cooler months may also occur. There is little evidence for a contribution of new particle formation



535 (although the summer season dataset is small), consistent with earlier work by Gani et al. (2020).  
536 Another notable feature is the apparent complexity and seasonal variability of sources of NO, NO<sub>2</sub>  
537 and BC, pollutants which can often be used to identify or locate sources of emissions. This is reflected  
538 in the various particle fractions, which generally correlate poorly with the other pollutants and with  
539 other than proximate size fractions.

540

541 The diurnal variation of all particle fractions is strongly suggestive of a road traffic influence,  
542 especially in the winter campaign. This appears strongly influenced by the emissions of heavy duty  
543 diesel traffic which is only able to access central Delhi at night. A size mode of <15 nm may well  
544 be attributable to vehicles using LPG/CNG fuels. However, the seasonal variability of the geographic  
545 distribution and wind speed dependence of sources revealed by the polar plots is strongly indicative  
546 of many other sources also contributing to all size fractions of particles.

547

#### 548 **DATA ACCESSIBILITY**

549 Data supporting this publication are openly available from the UBIRA eData repository at  
550 <https://doi.org/10.25500/edata.bham.00000730>

551

#### 552 **AUTHOR CONTRIBUTIONS**

553 This study was conceived by RMH. WJB managed the research programme, and MSA and LRC  
554 collected the data. DCB and UAS led the data analysis with contributions from JB and DB. UAS  
555 and RMH co-authored the first draft. ZS and all co-authors provided comments and revisions.

556

#### 557 **COMPETING INTERESTS**

558 The authors declare that they have no conflict of interest.

559

560



561 **FINANCIAL SUPPORT**

562 This research has been supported by the Natural Environment Research Council NE/P016499/1.

563

564 **ACKNOWLEDGEMENTS**

565 We are thankful the Scientific and Technical Research Council of Turkey (TUBITAK) (grant  
566 number 1059B191801445) to support the author Ulku Alver Sahin to work on the ASAP project.

567 We would also like to acknowledgement the IIT Delhi team under the Principal Investigator-ship of  
568 Professor Mukesh Khare who provided all the facilities including space and logistical help during  
569 the experiment.

570



571 **REFERENCES**

- 572  
573 Azimi, P., Zhao, D. and Stephens, B.: Estimates of HVAC filtration efficiency for fine and ultrafine  
574 particles of outdoor origin, *Atmos. Environ.*, 98, 337-346,  
575 <https://doi.org/10.1016/j.atmosenv.2014.09.007>, 2014.  
576  
577 Babu, S. S., Manoj, M.R., Moorthy, K. K., Mukunda, M. G., Vijayakumar, S.N., Sobhan, K.K.,  
578 Satheesh, S.K., Niranjan, K., Ramagopal, K., Bhuyan, P.K. and Singh, D.: Trends in aerosol optical  
579 depth over Indian region: Potential causes and impact indicators, *J. Geophys. Res.*, 118, 11794–  
580 11806, <https://doi.org/10.1002/2013JD020507>, 2013.  
581  
582 Balakrishnan, K., Pillarisetti, A., Yamanashita, K. and Yusoff, K.: Air Pollution in Asia and the  
583 Pasific: Science Based Solution, Published by the United Nations Environment Programme  
584 (UNEP), Chapter 1.2 Air quality and health in Asia and the Pacific, January 2019, ISBN: 978-92-  
585 807-3725-7, Bangkok, Thailand, 2019.  
586  
587 Beddows, D. C. S., Dall'osto, M. and Harrison, R. M.: An Enhanced Procedure for the Merging of  
588 Atmospheric Particle Size Distribution Data Measured Using Electrical Mobility and Time-of-  
589 Flight Analysers, *Aerosol Science and Technology*, 44, 11, 930-938,  
590 <https://doi.org/10.1080/02786826.2010.502159>, 2010.  
591  
592 Bhandari, S., Gani, S., Patel, K., Wang, D. S., Soni, P., Arub, Z., Habib, G., Apte, J.S. and Ruiz, L.  
593 H.: Sources and atmospheric dynamics of organic aerosol in New Delhi, India: insights from  
594 receptor modeling, *Atmos. Chem. Phys.*, 20, 735–752, <https://doi.org/10.5194/acp-20-735-2020>,  
595 2020.  
596  
597 Bikkina, S., Andersson, A., Kirillova, E. N., Holmstrand, H., Tiwari, S., Srivastava, A. K., Bisht,  
598 D.S. and Gustafsson, Ö.: Air quality in megacity Delhi affected by countryside biomass burning,  
599 *Nature Sustainability*, 2, 200–205, <https://doi.org/10.1038/s41893-019-0219-0>, 2019.  
600  
601 Bousiotis, D., Dall'Osto, M., Beddows, D. C. S., Pope, F. D., and Harrison, R. M.: Analysis of new  
602 particle formation (NPF) events at nearby rural, urban background and urban roadside sites, *Atmos.*  
603 *Chem. Phys.*, 19, 5679–5694, <https://doi.org/10.5194/acp-19-5679-2019>, 2019.  
604  
605 Bousiotis, D., Brean, J., Pope, F. D., Dall'Osto, M., Querol, X., Alastuey, A., Perez, N., Petäjä, T.,  
606 Massling, A., Nøjgaard, J. K., Nordstrøm, C., Kouvarakis, G., Vratolis, S., Eleftheriadis, K., Niemi,  
607 J. V., Portin, H., Wiedensohler, A., Weinhold, K., Merkel, M., Tuch, T., and Harrison, R. M.: The  
608 effect of meteorological conditions and atmospheric composition in the occurrence and  
609 development of new particle formation (NPF) events in Europe, *Atmos. Chem. Phys.*, 21, 3345–  
610 3370, <https://doi.org/10.5194/acp-21-3345-2021>, 2021.  
611  
612 Butt, E. W., Rap, A., Schmidt, A., Scott, C. E., Pringle, K. J., Reddington, C. L., Richards, N. A.  
613 D., Woodhouse, M. T., Ramirez-Villegas, J., Yang, H., Vakkari, V., Stone, E. A., Rupakheti, M., S.  
614 Praveen, P., G. van Zyl, P., P. Beukes, J., Josipovic, M., Mitchell, E. J. S., Sallu, S. M., Forster, P.  
615 M., and Spracklen, D. V.: The impact of residential combustion emissions on atmospheric aerosol,  
616 human health, and climate, *Atmos. Chem. Phys.*, 16, 873–905, [https://doi.org/10.5194/acp-16-873-](https://doi.org/10.5194/acp-16-873-2016)  
617 2016, 2016.  
618  
619 Casquero-Vera, J. A., Lyamani, H., Titos, G., Minguillón, M. C., Dada, L., Alastuey, A., Querol,  
620 X., Petäjä, T., Olmo, F. J. and Alados-Arboledas, L.: Quantifying traffic, biomass burning and  
621 secondary source contributions to atmospheric particle number concentrations at urban and



- 622 suburban sites, *Science of The Total Environment*, 768, 145282,  
623 doi.org/10.1016/j.scitotenv.2021.145282, 2021.
- 624
- 625 Chelani, A. B., Gajghate, D. G., ChalapatiRao, C. V. and Devotta, S.: Particle Size Distribution in  
626 Ambient Air of Delhi and Its Statistical Analysis, *Bull. Environ. Contam. Toxicol.*, 85, 22–27,  
627 https://doi.org/10.1007/s00128-010-0010-4, 2010.
- 628
- 629 Chen, F., Zhang, X., Zhu, X., Zhang, H., Gao, J. and Hopke, P. K.: Chemical Characteristics of  
630 PM<sub>2.5</sub> during a 2016 Winter Haze Episode in Shijiazhuang, China. *Aerosol Air Qual. Res.*, 17,  
631 368-380, <https://doi.org/10.4209/aaqr.2016.06.0274>, 2017.
- 632
- 633 Chowdhury, S., Dey, S., Tripathi, S. N., Beig, G., Mishra, A. K. and Sharma, S.:” Traffic  
634 intervention” policy fails to mitigate air pollution in megacity Delhi, *Environmental Science &*  
635 *Policy*, 74, 8-13, <https://doi.org/10.1016/j.envsci.2017.04.018>, 2017.
- 636
- 637 Conibear, L., Butt, E. W., Knotte, C., Arnold, S. R. and Spracklen, D. V.: Residential energy use  
638 emissions dominate health impacts from exposure to ambient particulate matter in Indi., *Nat.*  
639 *Commun.*, 9, 617, <https://doi.org/10.1038/s41467-018-02986-7>, 2018.
- 640
- 641 Cusworth, D. H., Mickley, L. J., Sulprizio, M. P., Liu, T., Marlier, M.E., DeFries, R. S.,  
642 Guttikunda, S.K. and Gupta, P.: Quantifying the influence of agricultural fires in northwest India on  
643 urban air pollution in Delhi, India, *Environ. Res. Lett.*, 13, 044018, <https://doi.org/10.1088/1748-9326/aab303>, 2018.
- 644
- 645
- 646 Dal Maso, M., Kulmala, M., Riipinen, I., Wagner, R., Hussein, T., Aalto, P. P. and Lehtinen, K. E.  
647 J.: Formation and growth of fresh atmospheric aerosols: eight years of aerosol size distribution data  
648 from SMEAR II, Hyytiälä, Finland, *Boreal Environmental Research* 10, 323-336, 2005.
- 649
- 650 Dandona, L., Dandona, R., Kumar, G. A., Shukla, D. K., Paul, V. K., Balakrishnan, K.,  
651 Prabhakaran, D., Tandon, N., Salvi, S., Dash, A. P., Nandakumar, A., Patel, V., Agarwal, S. K.,  
652 Gupta, P. C., Dhaliwal, R. S., Mathur, P., Laxmaiah, A., Dhillon, P. K., Dey, S., Mathur, M. R.,  
653 Afshin, A., Fitzmaurice, C., Gakidou, E., Gething, P., Hay, S.I., Kassebaum, N. J., Kyu, H., Lim, S.  
654 S., Naghavi, M., Roth, G. A., Stanaway, J. D., Whiteford, H., Chadha, V. K., Khaparde, S. D., Rao,  
655 R., Rade, K., Dewan, P., Furtado, M., Dutta, E., Varghese, C. M., Mehrotra, R., Jambulingam, P.,  
656 Kaur, T., Sharma, M., Singh, S., Arora, R., Rasaily, R., Anjana, R. M., Mohan, V., Agrawal, A.,  
657 Chopra, A., Mathew, A. J., Bhardwaj, D., Muraleedharan, P., Mutreja, P., Bienhoff, K., Glenn, S.,  
658 Abdulkader, R. S., Aggarwal, A. N., Aggarwal, R., Albert, S., Ambekar, A., Arora, M., Bachani,  
659 D., Bavdekar, A., Beig, G., Bhansali, A., Bhargava, A., Bhatia, E., Camara, B., Christopher, D. J.,  
660 Das, S. K., Dave, P. V., Dey, S., Ghoshal, A. G., Gopalakrishnan, N., Guleria, R., Gupta, R., Gupta,  
661 S. S., Gupta, T., Gupte, M. D., Gururaj, G., Harikrishnan, S., Iyer, V., Jain, S.K., Jeemon, P.,  
662 Joshua, V., Kant, R., Kar, A., Kataki, A.C., Katoch, K., Khera, A., Kinra, S., Koul, P.A., Krishnan,  
663 A., Kumar, A., Kumar, R. K., Kumar, R., Kurpad, A., Ladusingh, L., Lodha, R., Mahesh, P. A.,  
664 Malhotra, R., Mathai, M., Mavalankar, D., Mohan Bv, M., Mukhopadhyay, S., Murhekar, M.,  
665 Murthy, G.V.S., Nair, S., Nair, S. A., Nanda, L., Nongmaithem, R. S., Oommen, A.M., Pandian,  
666 J.D., Pandya, S., Parameswaran, S., Pati, S., Prasad, K., Prasad, N., Purwar, M., Rahim, A., Raju,  
667 S., Ramji, S., Rangaswamy, T., Rath, G. K., Roy, A., Sabde, Y., Sachdeva, K. S., Sadhu, H., Sagar,  
668 R., Sankar, M. J., Sharma, R., Shet, A., Shirude, S., Shukla, R., Shukla, S. R., Singh, G., Singh, N.  
669 P., Singh, V., Sinha, A., Sinha, D. N., Srivastava, R. K., Srividya, A., Suri, V., Swaminathan, R.,  
670 Sylaja, P. N., Tandale, B., Thakur, J. S., Thankappan, K.R., Thomas, N., Tripathy, S., Varghese,  
671 M., Varughese, S., Venkatesh, S., Venugopal, K., Vijayakumar, L., Xavier, D., Yajnik, C. S.,  
672 Zachariah, G., Zodpey, S., Rao, J. V. R. P., Vos, T., Reddy, K. S., Murray, C. J. L. and  
673 Swaminathan, S.: Nations within a nation: variations in epidemiological transition across the states



- 674 of India, 1990-2016 in the global burden of disease study. *The Lancet*, 390, 10111, 2437-2460,  
675 [https://doi.org/10.1016/S0140-6736\(17\)32804-0](https://doi.org/10.1016/S0140-6736(17)32804-0), 2017.
- 676
- 677 Das, A., Kumar, A., Habib, G. and Vivekanandan, P.: Insights on the biological role of ultrafine  
678 particles of size  $PM_{<0.25}$ : A prospective study from New Delhi, *Environmental Pollution*, 268, Part  
679 B, 115638, <https://doi.org/10.1016/j.envpol.2020.115638>, 2021.
- 680
- 681 DeCarlo, P. F., Slowik, J. G., Worsnop, D. R., Davidovits, P. and Jimenez, J. L.: Particle  
682 Morphology and Density Characterization by Combined Mobility and Aerodynamic Diameter  
683 Measurements. Part 1: Theory, *Aerosol Science and Technology*, 38:12, 1185-  
684 1205, <https://doi.org/10.1080/027868290903907>, 2004.
- 685
- 686 Dhyani, R., Sharma, N. and Advani, M.: Estimation of Fuel Loss and Spatial-Temporal Dispersion  
687 of Vehicular Pollutants at a Signalized Intersection in Delhi City, India. *WIT Transaction on  
688 Ecology and the Environment: Air Pollution 2019*, WIT Press, 236, 233-247, ISBN: 978-1-78466-  
689 343-8, Editor: Passerini et al., 2019.
- 690
- 691 Dumka, U. C., Tiwari, S., Kaskaoutis, D. G., Soni, V. K., Safai, P. D. and Attri, S. D.: Aerosol and  
692 pollutant characteristics in Delhi during a winter research campaign, *Environ. Sci. Pollut. Res.*, 26,  
693 3771–3794. <https://doi.org/10.1007/s11356-018-3885-y>, 2019.
- 694
- 695 Gani S., Bhandari, S., Patel, K., Seraj, S., Soni, P., Arub, Z., Habib, G., Ruiz, L.H. and Apte, J.S.:  
696 Particle number concentrations and size distribution in a polluted megacity: the Delhi Aerosol  
697 Supersite study, *Atmos. Chem. Phys.*, 20, 8533–8549, <https://doi.org/10.5194/acp-20-8533-2020>,  
698 2020.
- 699
- 700 Giechaskiel, B., Lähde, T. and Drossinos, Y. Regulating particle number measurements from the  
701 tailpipe of light-duty vehicles: The next step?, *Environmental Research*, 172, 1-9,  
702 <https://doi.org/10.1016/j.envres.2019.02.006>, 2019.
- 703
- 704 Gulia, S., Shiva Nagendra, S.M., Khare, M. and Khanna, I.: Urban air quality management-A  
705 review, *Atmospheric Pollution Research*, 6, 2, 286-304, <https://doi.org/10.5094/APR.2015.033>,  
706 2015.
- 707
- 708 Guo, H., Kota, S.H., Sahu, S.K., Hu, J., Ying, Q., Gao, A. and Zhang, H.: Source apportionment of  
709  $PM_{2.5}$  in North India using source-oriented air quality models, *Environmental Pollution*, 231, 1,  
710 426-436, <https://doi.org/10.1016/j.envpol.2017.08.016>, 2017.
- 711
- 712 Gupta, S., Kumar, K., Srivastava, A., Srivastava, A. and Jain, V. K.: Size distribution and source  
713 apportionment of polycyclic aromatic hydrocarbons (PAHs) in aerosol particle samples from the  
714 atmospheric environment of Delhi, India, *Science of The Total Environment*, 409, 22, 4674-4680,  
715 <https://doi.org/10.1016/j.scitotenv.2011.08.008>, 2011.
- 716
- 717 Gurjar, B. R., van Aardenne, J. A., Lelieveld, J. and Mohan, M.: Emission estimates and trends  
718 (1990–2000) for megacity Delhi and implications, *Atmospheric Environment*, 38, 33, 5663-5681,  
719 <https://doi.org/10.1016/j.atmosenv.2004.05.057>, 2004.
- 720
- 721 Guttikunda, S. K., Goel, R. and Pant, P.: Nature of air pollution, emission sources, and management  
722 in the Indian cities, *Atmospheric Environment*, 95, 501-510,  
723 <https://doi.org/10.1016/j.atmosenv.2014.07.006>, 2014.



- 724 Guttikunda, S.K. and Gurjar, B.R.: Role of meteorology in seasonality of air pollution in megacity  
725 Delhi, India, *Environ. Monit. Assess.*, 184, 3199–3211. <https://doi.org/10.1007/s10661-011-2182-8>,  
726 2012.  
727
- 728 Hama, S.M.L., Kumar, P., Harrison, R.M., Bloss, W.J., Khare, M., Mishra, S., Namdeo, A., Sokhi,  
729 R., Goodman, P. and Sharma, C.: Four-year assessment of ambient particulate matter and trace  
730 gases in the Delhi-NCR region of India, *Sustainable Cities and Society*, 54, 102003,  
731 <https://doi.org/10.1016/j.scs.2019.102003>, 2020.  
732
- 733 Hama, S.M.L., Cordell, R. L. and Monks, P. S.: Quantifying primary and secondary source  
734 contributions to ultrafine particles in the UK urban background, *Atmos. Environ.*, 166, 62–78,  
735 [doi.org/10.1016/j.atmosenv.2017.07.013](https://doi.org/10.1016/j.atmosenv.2017.07.013), 2017.  
736
- 737 Hamed, A., Joutsensaari, J., Mikkonen, S., Sogacheva, L., Dal Maso, M., Kulmala, M., Cavalli, F.,  
738 Fuzzi, S., Facchini, M. C., Decesari, S., Mircea, M., Lehtinen, K. E. J., and Laaksonen, A.:  
739 Nucleation and growth of new particles in Po Valley, Italy, *Atmos. Chem. Phys.*, 7, 355–376,  
740 <https://doi.org/10.5194/acp-7-355-2007>, 2007.  
741
- 742 Han, Y., Iwamoto, Y., Nakayama, T., Kawamura, K., Hussein, T. and Mochida, M.: Observation of  
743 new particle formation over a mid-latitude forest facing the North Pacific, *Atmos. Environ.*, 64, 77–  
744 84, <https://doi.org/10.1016/j.atmosenv.2012.09.036>, 2013.  
745
- 746 Harrison R.M.: Airborne particulate matter, *Phil. Trans. R. Soc. A*, 378, 20190319.  
747 <http://dx.doi.org/10.1098/rsta.2019.0319>, 2020.  
748
- 749 Harrison, R. M., Rob MacKenzie, A., Xu, H., Alam, M. S., Nikolova, I., Zhong, J., ... and Liang, Z.,  
750 Diesel exhaust nanoparticles and their behaviour in the atmosphere. *Proceedings of the Royal*  
751 *Society A*, 474(2220), 20180492, 2018.  
752
- 753 Harrison, R. M., Beddows, D.C.S. and Dall'Osto, M.: PMF Analysis of Wide-Range Particle Size  
754 Spectra Collected on a Major Highway, *Environ. Sci. Technol.*, 45, 13, 5522–5528,  
755 <https://doi.org/10.1021/es2006622>, 2011.  
756
- 757 Jain, S., Sharma, S. K., Vijayan, N., Mandal, T. K.: Seasonal characteristics of aerosols (PM<sub>2.5</sub> and  
758 PM<sub>10</sub>) and their source apportionment using PMF: A four year study over Delhi, India,  
759 *Environmental Pollution*, 262, 114337, <https://doi.org/10.1016/j.envpol.2020.114337>, 2020.  
760
- 761 Jeong, C.H., Evans, G. J., McGuire, M. L., Chang, R. Y.W. and Abbatt, J. P. D.: Zeromskiene, K.,  
762 Mozurkewich, M., Li, S.-M., and Leitch, W. R.: Particle formation and growth at five rural and  
763 urban sites, *Atmos. Chem. Phys.*, 10, 7979–7995, <https://doi.org/10.5194/acp-10-7979-2010>, 2010.  
764
- 765 Jing, H., Li, Y.F., Zhao, J., Li, B., Sun, J., Chen, R., Gao, Y. and Chen, C.: Wide-range particle  
766 characterization and elemental concentration in Beijing aerosol during the 2013 Spring Festival,  
767 *Environmental Pollution*, 192, 204–211, <https://doi.org/10.1016/j.envpol.2014.06.003>, 2014.  
768
- 769 Kalafut-Pettibone, A. J., Wang, J., Eichinger, W. E., Clarke, A., Vay, S. A., Blake, D. R., and  
770 Stanier, C. O.: Size-resolved aerosol emission factors and new particle formation/growth activity  
771 occurring in Mexico City during the MILAGRO 2006 Campaign, *Atmos. Chem. Phys.*, 11, 8861–  
772 8881, <https://doi.org/10.5194/acp-11-8861-2011>, 2011.  
773



- 774 Kanawade, V.P., Srivastava, A.K., Ram, K., Asmi, E., Vakkari, V., Soni, V.K., Varaprasad, V. and  
775 Sarangi, C.: What caused severe air pollution episode of November 2016 in New Delhi?, *Atmos.*  
776 *Environ.*, 222, 117125, <https://doi.org/10.1016/j.atmosenv.2019.117125>, 2020.  
777
- 778 Kontses, A., Triantafyllopoulos, G., Ntziachristos, L. and Samaras, Z.: Particle number (PN)  
779 emissions from gasoline, diesel, LPG, CNG and hybrid-electric light-duty vehicles under real-world  
780 driving conditions, *Atmos. Environ.*, 222, 117126, <https://doi.org/10.1016/j.atmosenv.2019.117126>,  
781 2020.  
782
- 783 Kuang, C., Chen, M., Zhao, J., Smith, J., McMurry, P. H., and Wang, J.: Size and time-resolved  
784 growth rate measurements of 1 to 5 nm freshly formed atmospheric nuclei, *Atmos. Chem. Phys.*,  
785 12, 3573–3589, <https://doi.org/10.5194/acp-12-3573-2012>, 2012.  
786
- 787 Kulmala, M., Dada, L., Daellenbach, K.r., Yan, C., Stolzenburg, D., Kontkanen, J., Ezhova, E.,  
788 Hakala, S., Tuovinen, S., Kokkonen, T.V., Kurpp, M., Cai, R., Zhou, Y., Yin, R., Baalbaki, R.,  
789 Chan, T., Chu, B., Deng, C., Fu, Y., Ge, M., He, H., Heikkinen, L., Junninen, H., Liu, Y., Lu, Y.,  
790 Nie, W., Rusanen, A., Vakkari, V., Wang, Y., Yang, G., Yao, L., Zheng, J., Kujansuu, J.,  
791 Kangasluoma, J., Petäjä, T., Paasonen, P., Järvi, L., Worsnop, D., Ding, A., Liu, Y., Wang, L.,  
792 Jiang, J., Bianchi, F. and Kerminen, V.M.: Is reducing new particle formation a plausible solution to  
793 mitigate particulate air pollution in Beijing and other Chinese megacities? *Faraday Discussion* 226,  
794 221, [doi.org/10.1039/D0FD00078G](https://doi.org/10.1039/D0FD00078G), 2021.  
795
- 796 Kulmala M., Luoma K., Virkkula A., Petäjä T., Paasonen P., Kerminen V.-M., Nie W., Qi X., Shen  
797 Y., Chi X. and Ding A.: On the mode-segregated aerosol particle number concentration load:  
798 contributions of primary and secondary particles in Hyytiälä and Nanjing. *Boreal, Env. Res.*, 21,  
799 319–331. 2016.  
800
- 801 Kumar, A., Ambade, B., Sankar, T. K., Sethi, S. S. and Kurwadkar, S.: Source identification and  
802 health risk assessment of atmospheric PM<sub>2.5</sub>-bound polycyclic aromatic hydrocarbons in  
803 Jamshedpur, India, *Sustainable Cities and Society*, 52, 101801,  
804 <https://doi.org/10.1016/j.scs.2019.101801>, 2020.  
805
- 806 Kumar, P., Gulia, S., Harrison, R. M. and Khare, M.: The influence of odd–even car trial on fine  
807 and coarse particles in Delhi, *Environmental Pollution*, 225, 20-30,  
808 <https://doi.org/10.1016/j.envpol.2017.03.017>, 2017.  
809
- 810 Kumar, P., Pirjola, L., Ketzel, M., and Harrison, R. M.: Nanoparticle emissions from 11 non-  
811 vehicle exhaust sources – A review, *Atmos. Environ.*, 67, 252–277,  
812 <https://doi.org/10.1016/j.atmosenv.2012.11.011>, 2013.  
813
- 814 Iida, K., Stolzenburg, M.R., McMurry, P.H. and Smith, J.N.: Estimating nanoparticle growth rates  
815 from size-dependent charged fractions: Analysis of new particle formation events in Mexico City,  
816 *J. Geophys. Res.*, 113, D05207, [doi.org/10.1029/2007JD009260](https://doi.org/10.1029/2007JD009260), 2008  
817
- 818 Liu, J., Jiang, J., Zhang, Q., Deng, J., and Hao, J.: A spectrometer for measuring particle size  
819 distributions in the range of 3 nm to 10 μm, *Front. Environ. Sci. Eng.*, 10, 63–72,  
820 <https://doi.org/10.1007/s11783-014-0754-x>, 2016.  
821
- 822 Magara-Gomez, K.T., Olson, M.R., McGinnis, J.E., Zhang, M. and Schauer, J.J.: Effect of Ambient  
823 Temperature and Fuel on Particle Number Emissions on Light-Duty Spark-Ignition Vehicles,  
824 *Aerosol Air Qual. Res.*, 14, 1360-1371. <https://doi.org/10.4209/aaqr.2013.06.0183>, 2014.  
825



- 826 Mahato, S., Pal, S. and Ghosh, K. G.: Effect of lockdown amid COVID-19 pandemic on air quality  
827 of the megacity Delhi, India, *Science of The Total Environment*, 730, 139086,  
828 <https://doi.org/10.1016/j.scitotenv.2020.139086>, 2020.  
829
- 830 Masiol, M., Vu, T. V., Beddows, D. C. S. and Harrison, R. M.: Source apportionment of wide range  
831 particle size spectra and black carbon collected at the airport of Venice (Italy), *Atmospheric*  
832 *Environment*, 139, 56-74, <https://doi.org/10.1016/j.atmosenv.2016.05.018>, 2016.  
833
- 834 Mönkkönen, P., Koponen, I. K., Lehtinen, K. E. J., Hämeri, K., Uma, R., and Kulmala, M.:  
835 Measurements in a highly polluted Asian mega city: observations of aerosol number size  
836 distribution, modal parameters and nucleation events, *Atmos. Chem. Phys.*, 5, 57–66,  
837 <https://doi.org/10.5194/acp-5-57-2005>, 2005.  
838
- 839 Nagpure, A.S., Ramaswami, A. and Russell, A.: Characterizing the Spatial and Temporal Patterns  
840 of Open Burning of Municipal Solid Waste (MSW) in Indian Cities, *Environ. Sci. Technol.*, 49, 21,  
841 12904–12912, <https://doi.org/10.1021/acs.est.5b03243>, 2015.  
842
- 843 Narain, U. and Krupnick, A., The Impact of Delhi's CNG Program on Air Quality. RFF Discussion  
844 Paper No. 07-06, Available at  
845 SSRN: <https://ssrn.com/abstract=969727> or <http://dx.doi.org/10.2139/ssrn.969727>, 2007.  
846
- 847 Ondráček, J., Ždímal, V., Smolík, J., and Lazaridis, M.: A Merging Algorithm for Aerosol Size  
848 Distribution from Multiple Instruments, *Water Air Soil Pollut.*, 199, 219–233,  
849 <https://doi.org/10.1007/s11270-008-9873-y>, 2009.  
850
- 851 Pant, P. and Harrison, R. M.: Critical Review of Receptor Modelling for Particulate Matter: A Case  
852 Study of India, *Atmos. Environ.*, 49, 1-12, <https://doi.org/10.1016/j.atmosenv.2011.11.060>, 2012.  
853
- 854 Pant, P., Baker, S. J., Goel, R., Guttikunda, S., Goel, A., Shukla, A. and Harrison, R.M.: Analysis of  
855 size-segregated winter season aerosol data from New Delhi, India, *Atmos. Poll. Res.*, 7, 1, 100-109,  
856 <https://doi.org/10.1016/j.apr.2015.08.001>, 2016.  
857
- 858 R Core Team, 2015. R: a Language and Environment for Statistical Computing. R Foundation for  
859 Statistical Computing, Vienna, Austria. <http://www.R-project.org/>.  
860
- 861 Rai, P., Furger, M., Haddad, I.E., Kumar, V., Wang, L., Singh, A., Dixit, K., Bhattu, D., Petit, J.E.,  
862 Ganguly, D., Rastogi, N., Baltensperger, U., Tripathi, S.N., Slowik, J.G. and Prévôt, A.S.H.: Real-  
863 time measurement and source apportionment of elements in Delhi's atmosphere, *Science of The*  
864 *Total Environment*, 742, 140332, <https://doi.org/10.1016/j.scitotenv.2020.140332>, 2020.  
865
- 866 Rodríguez, S. and Cuevas, E.: The contributions of “minimum primary emissions” and “new  
867 particle formation enhancements” to the particle number concentration in urban air, *Journal of*  
868 *Aerosol Science* 38, 1207-1219, <https://doi.org/10.1016/j.jaerosci.2007.09.001>, 2007.  
869
- 870 Rodríguez-Urrego, D. and Rodríguez-Urrego, L.: Air quality during the COVID-19: PM2.5 analysis  
871 in the 50 most polluted capital cities in the world, *Environmental Pollution*, 266, 1, 115042,  
872 <https://doi.org/10.1016/j.envpol.2020.115042>, 2020.  
873
- 874 Salvador, P., Barreiro, M., Gómez-Moreno, F. J., Alonso-Blanco, E. and Artúñano, B.: Synoptic  
875 classification of meteorological patterns and their impact on air pollution episodes and new particle  
876 formation processes in a south European air basin, *Atmos.c Environ.*, 245, 118016,  
877 <https://doi.org/10.1016/j.atmosenv.2020.118016>, 2021.



- 878 Sarangi, B., Aggarwal, S. G., and Gupta, P. K.: A simplified approach to calculate particle growth  
879 rate due to self-coagulation, scavenging and condensation using SMPS measurements during a  
880 particle growth event in New Delhi, *Aerosol and air quality research*, 15(1), 166-179, [https://doi:  
881 10.4209/aaqr.2013.12.0350](https://doi.org/10.4209/aaqr.2013.12.0350), 2015.  
882
- 883 Sarangi, B., Aggarwal, S. G., Kunwar, B., Kumar, S., Kaur, R., Sinha, D., Tiwari, S. and  
884 Kawamura, K.: Nighttime particle growth observed during spring in New Delhi: Evidences for the  
885 aqueous phase oxidation of SO<sub>2</sub>, *Atmospheric environment*, 188, 82-96,  
886 <https://doi.org/10.1016/j.atmosenv.2018.06.018>, 2018  
887
- 888 Schmid, O., Karg, E., Hagen, D. E., Whitefield, P. D. and Ferron, G. A.: On the Effective Density  
889 of Non-Spherical Particles as Derived From Combined Measurements of Aerodynamic and  
890 Mobility Equivalent Size, *Atmos. Environ.*, 38, 431–443.  
891 <https://doi.org/10.1016/j.jaerosci.2007.01.002>, 2007.  
892
- 893 Schreiber, D., Forss, A. M., Mohr, M. and Dimopoulos, P.: Particle Characterisation of Modern  
894 CNG, Gasoline and Diesel Passenger Cars, 8th International Conference on Engines for  
895 Automobiles, Technical Paper 2007-24-0123, ISSN: 0148-7191, e-ISSN: 2688-3627,  
896 <https://doi.org/10.4271/2007-24-0123>, 2007.  
897
- 898 Tiwari, S., Bisht, D.S., Srivastava, A.K., Pipal, A.S., Taneja, A., Srivastava, M.K. and Attri, S.D.:  
899 Variability in atmospheric particulates and meteorological effects on their mass concentrations over  
900 Delhi, India, *Atmospheric Research*, 145–146, 45-56,  
901 <https://doi.org/10.1016/j.atmosres.2014.03.027>, 2014.  
902
- 903 Toumasatos, Z., Kontses, A., Doulgeris, S., Samaras, Z. and Ntziachristos, L.: Particle emissions  
904 measurements on CNG vehicles focusing on Sub-23nm, *Aerosol Science and Technology*, 55,  
905 2, 182-193, <https://doi.org/10.1080/02786826.2020.1830942>, 2021.  
906
- 907 Tyagi, S., Tiwari, S., Mishra, A., Hopke, P.K., Attri, S.D., Srivastava, A.K. and Bisht, D. S.: Spatial  
908 variability of concentrations of gaseous pollutants across the National Capital Region of Delhi,  
909 India, *Atmospheric Pollution Research*, 7, 5, 808-816, <https://doi.org/10.1016/j.apr.2016.04.008>,  
910 2016.  
911
- 912 Vu, T. V., Delgado-Saborit, J. M. and Harrison, R. M.: Particle number size distributions from  
913 seven major sources and implications for source apportionment studies. *Atmospheric Environment*,  
914 122, 114-132, <https://doi.org/10.1016/j.atmosenv.2015.09.027>, 2015.  
915
- 916 Wu, T. and Boor, B. E.: Urban aerosol size distributions: a global perspective, *Atmos. Chem. Phys.*,  
21, 8883–8914, <https://doi.org/10.5194/acp-21-8883-2021>, 2021.  
917
- 918 Yadav, R., Sahu, L.K., Beig, G. and Jaaffrey, S.N.A.: Role of long-range transport and local  
919 meteorology in seasonal variation of surface ozone and its precursors at an urban site in India,  
920 *Atmospheric Research*, 176–177, 96-107, <https://doi.org/10.1016/j.atmosres.2016.02.018>, 2016.  
921
- 922 Zhang, Y. M., Zhang, X. Y., Sun, J. Y., Lin, W. L., Gong, S. L., Shen, X. J. and Yang, S.:  
923 Characterization of new particle and secondary aerosol formation during summertime in Beijing,  
924 China, *Tellus B: Chemical and Physical Meteorology*, 63:3, 382-394,  
925 <https://doi.org/10.1111/j.1600-0889.2011.00533.x>, 2011.  
926
- 927 Zhu, C., Li, J.G., Wang, L., Morawska, L., Zhang, X. and Zhang, Y.L.: Size-resolved particle  
928 distribution and gaseous concentrations by real-world road tunnel measurement, *Indoor and Built  
929 Environment*, 23, 2, 225-235, <https://doi.org/10.1177/1420326X13509290>, 2014.



930 **FIGURE CAPTIONS:**

931

932 **Figure 1.** Comparison of average particle number counts ( $\#/cm^3$ ) for nucleation, aitken,  
933 accumulation, large fine and coarse modes of PM between 15 nm and 10  $\mu m$  in all  
934 seasons, and the volume contributions for comparison.

935

936 **Figure 2.** Average diurnal variation of particle number counts for nucleation, Aitken,  
937 accumulation, large fine and coarse modes and  $PM_{2.5}$ , BC, NO and  $NO_2$  in autumn,  
938 summer and winter.

939

940 **Figure 3.** Average diurnal variation of total particle number counts (between 15 and 10  $\mu m$ ) for  
941 weekday average (Monday to Friday), Saturday and Sunday in Delhi. (Summer data  
942 are very limited. There are no data on Friday afternoon, night and Saturday early  
943 morning (Figure S6)).

944

945 **Figure 4.** Diurnal contour plots for particles derived by SMPS between 15 and 660 nm averaged  
946 for each season (a: winter, b: Autumn and c: Summer) and for 3 June 2018 data when  
947 a NPF event probably occurred (d), the solid line showing the  $NO_x$  mixing ratio. Note  
948 the different scales for the seasons presented.

949

950 **Figure 5.** The hourly average of day and night particle numbers for all modes from the wide  
951 range particle sizes derived from the merged data.  $UFP = \text{Nucleation} + \text{Aitken}$ ,  $PN_1 =$   
952  $UFP + \text{Accumulation}$ ,  $PN_{10} = PN_1 + \text{Large Fine} + \text{Coarse}$ .

953

954 **Figure 6.** Seasonal average (line) and standard deviation (shadow) of particle number size  
955 distributions.

956

957 **Figure 7.** Hourly average day and night (left side) and during day hours (right side) particle  
958 number distributions in autumn, summer and winter in Delhi.

959

960 **Figure 8.** Diurnal change of the geometric mean diameter (GMD) calculated for winter, autumn  
961 and summer seasons. Growth rates (nm/hour) are calculated from  $dGMD/dt$ .

962

963 **Figure 9.** Hourly average particle number, volume and area distributions in the winter (a),  
964 autumn (b) and summer (c) in Delhi.

965

966 **Figure 10.** Correlation coefficient (R) between the hourly average PNs of five particle size  
967 fractions (left side) and NO,  $NO_2$ , BC (right side).

968

969 **Figure 11.** Polar plots of PNs ( $\#/cm^3$ ) for five particle size fractions in winter, autumn and  
970 summer in Delhi.

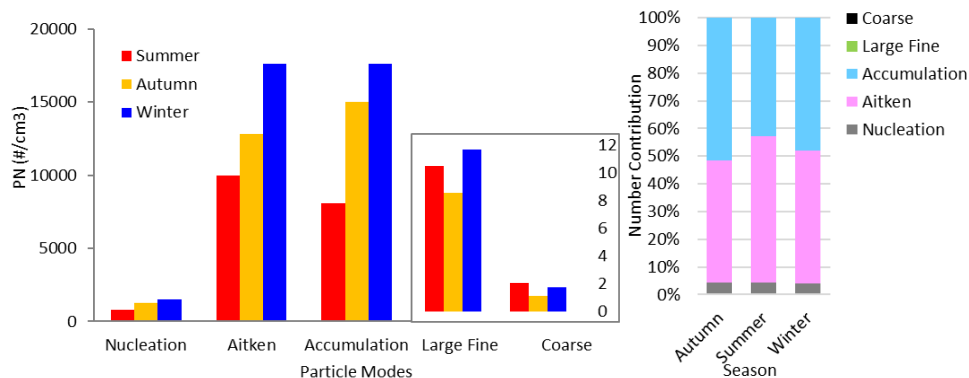
971

972

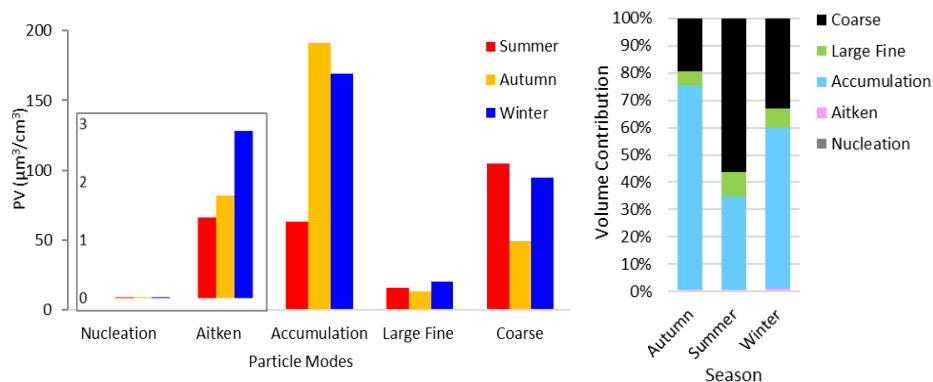
973



974



975



976

977

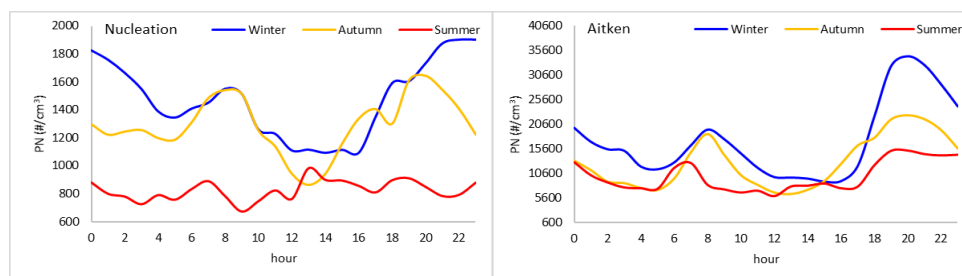
978 **Figure 1.** Comparison of average particle number counts (#/cm<sup>3</sup>) for nucleation, aitken,  
 979 accumulation, large fine and coarse modes of PM between 15 nm and 10 μm in all seasons, and the  
 980 volume contributions for comparison.

981

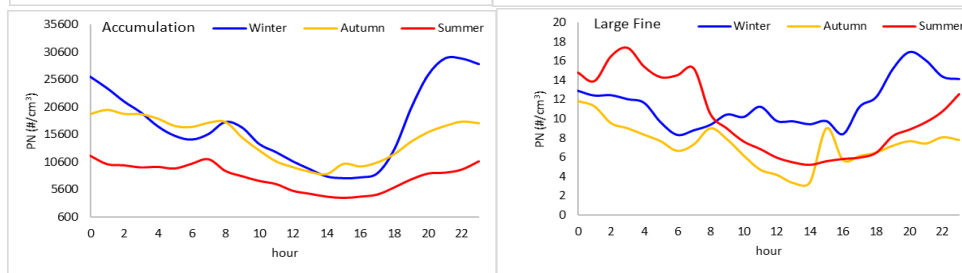
982



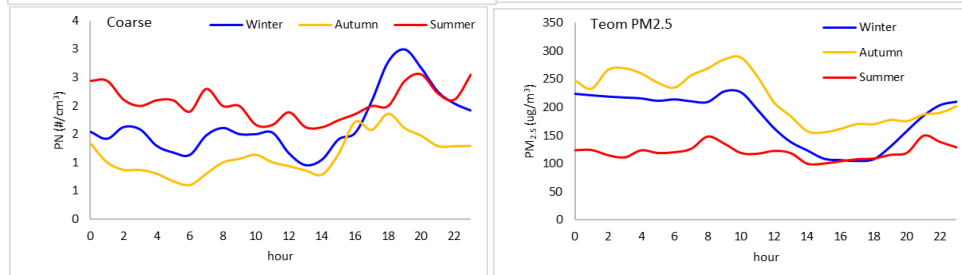
983



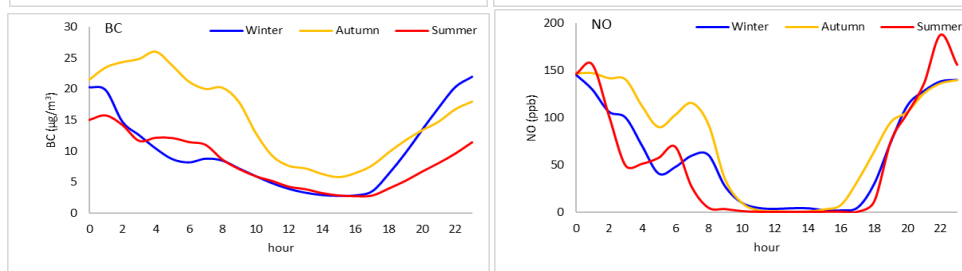
984



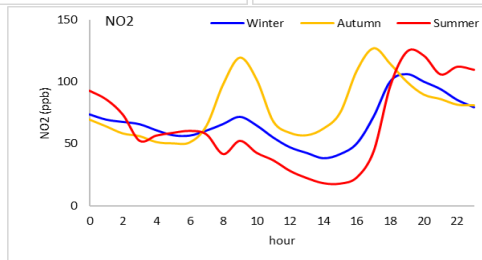
985



986



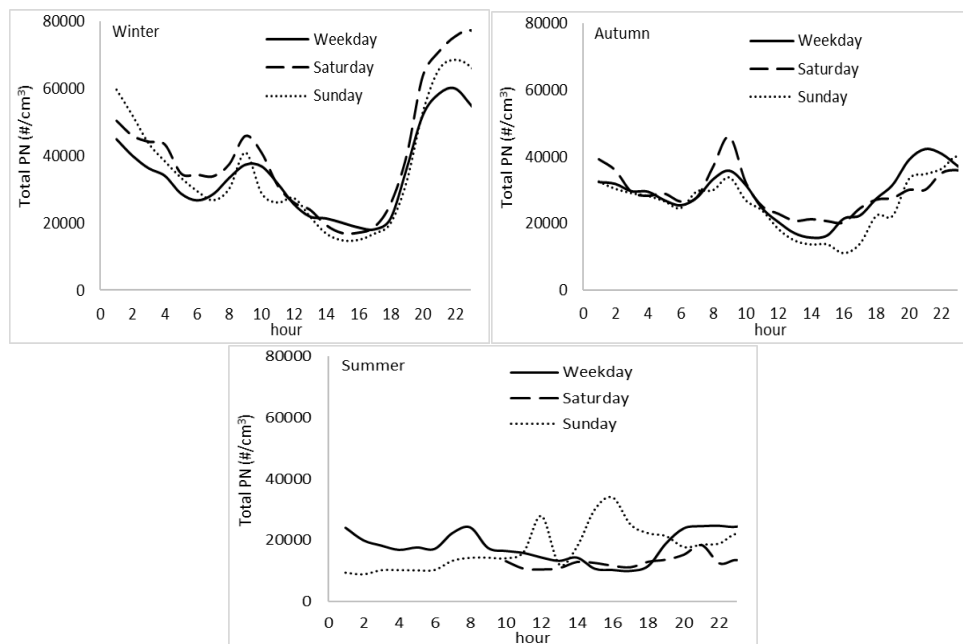
987



988 **Figure 2.** Average diurnal variation of particle number counts for nucleation, Aitken, accumulation,  
989 large fine and coarse modes and PM<sub>2.5</sub>, BC, NO and NO<sub>2</sub> in autumn, summer and winter.  
990



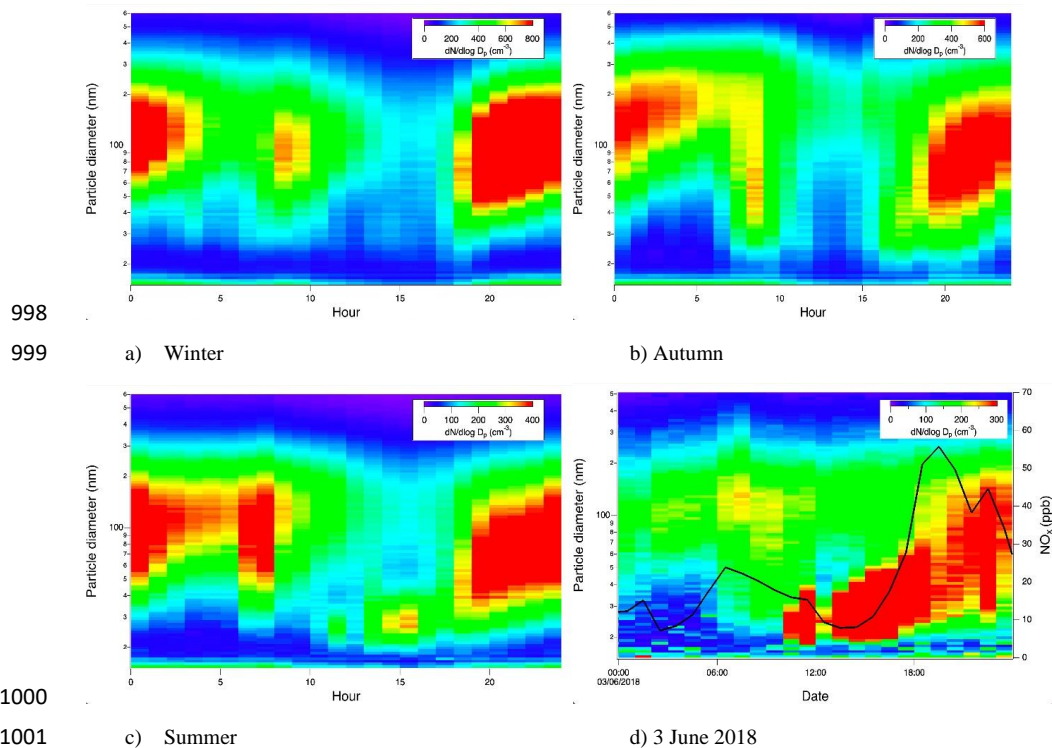
991



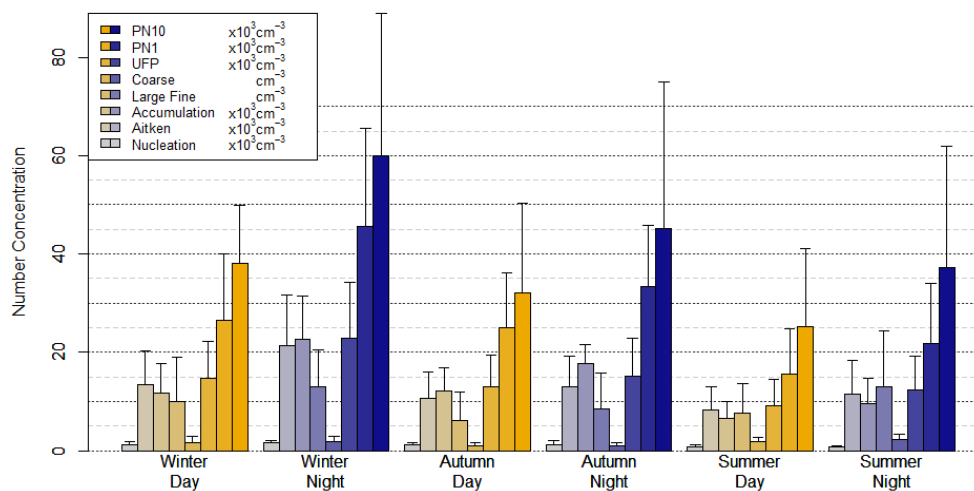
992

993

994 **Figure 3.** Average diurnal variation of total particle number counts (between 15 and 10  $\mu\text{m}$ ) for  
995 weekday average (Monday to Friday), Saturday and Sunday in Delhi. (Summer data are very  
996 limited. There are no data on Friday afternoon, night and Saturday early morning (Figure S6)).  
997

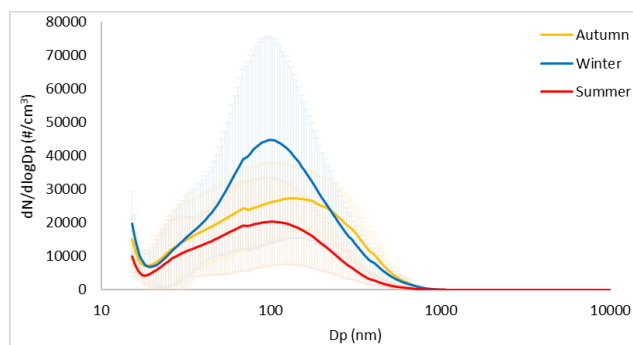


1003 **Figure 4.** Diurnal contour plots for particles derived by SMPS between 15 and 660 nm averaged for  
1004 each season (a: winter, b: Autumn and c: Summer) and for 3 June 2018 data when a NPF event  
1005 probably occurred (d), the solid line showing the  $\text{NO}_x$  mixing ratio. Note the different scales for the  
1006 seasons presented.  
1007



1008  
1009  
1010  
1011  
1012

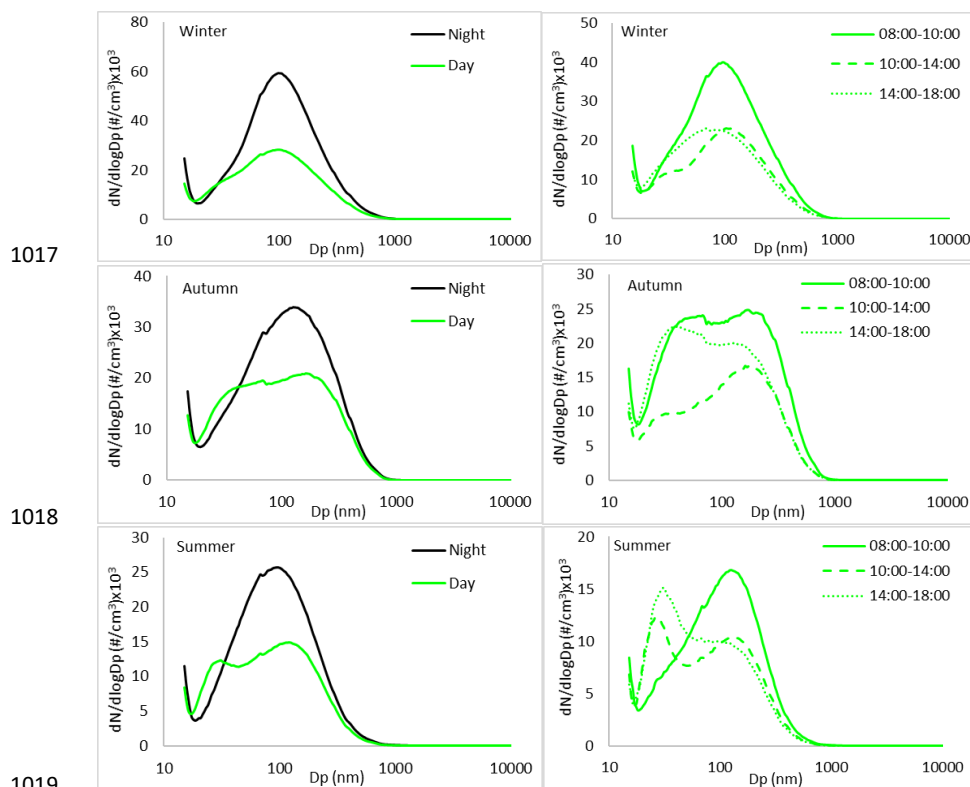
**Figure 5.** The hourly average of day and night particle numbers for all modes from the wide range particle sizes derived from the merged data. UFP =Nucleation +Aitken, PN<sub>1</sub> = UFP+Accumulation, PN<sub>10</sub>= PN<sub>1</sub>+Large Fine+Coarse.



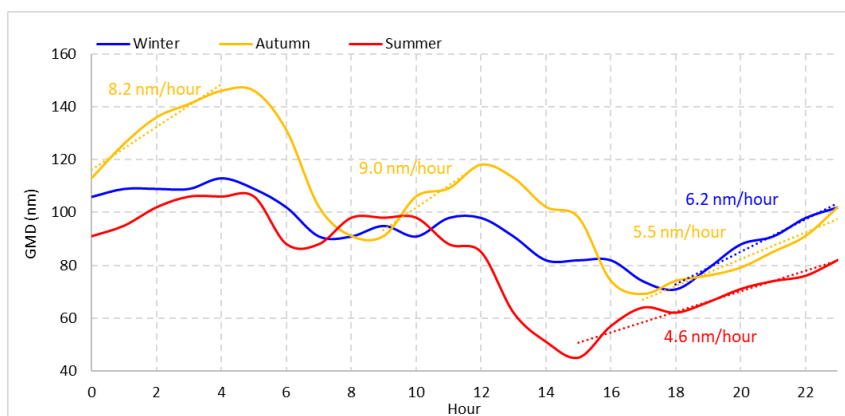
1013

1014 **Figure 6.** Seasonal average (line) and standard deviation (shadow) of particle number size  
1015 distributions.

1016



1020 **Figure 7.** Hourly average day and night (left side) and during day hours (right side) particle number  
1021 distributions in autumn, summer and winter in Delhi.  
1022



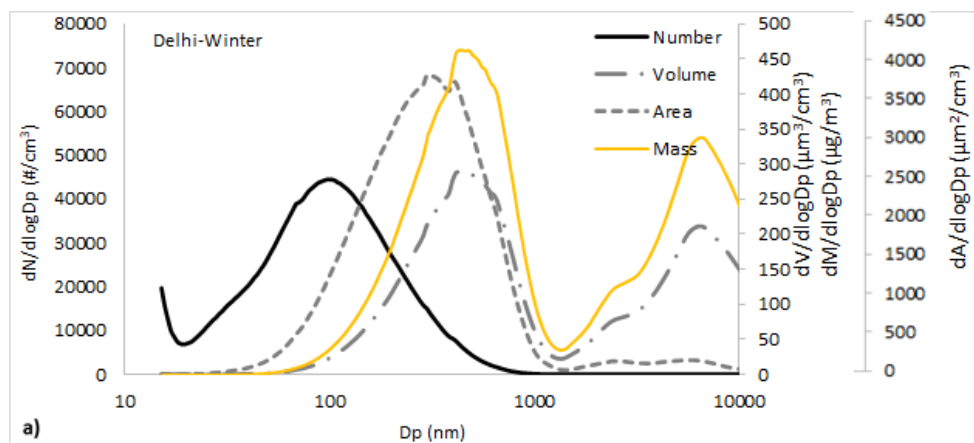
1023

1024 **Figure 8.** Diurnal change of the geometric mean diameter (GMD) calculated for winter, autumn  
1025 and summer seasons. Growth rates (nm/hour) are calculated from  $dGMD/dt$ .

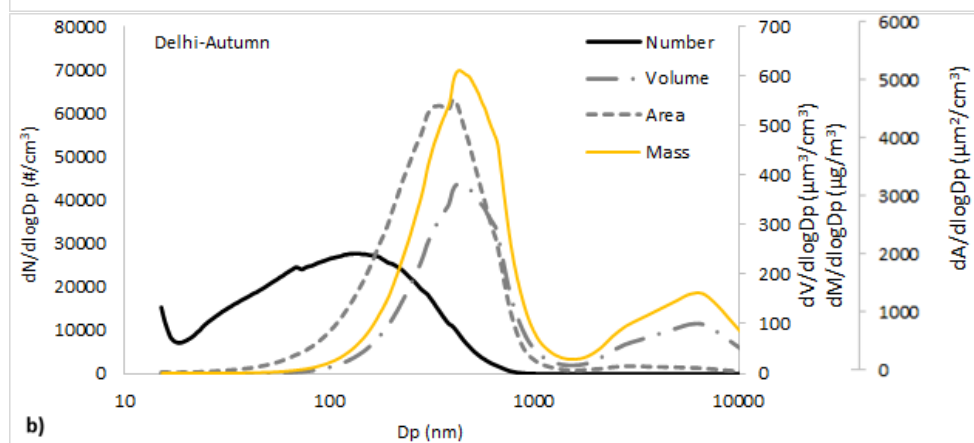
1026



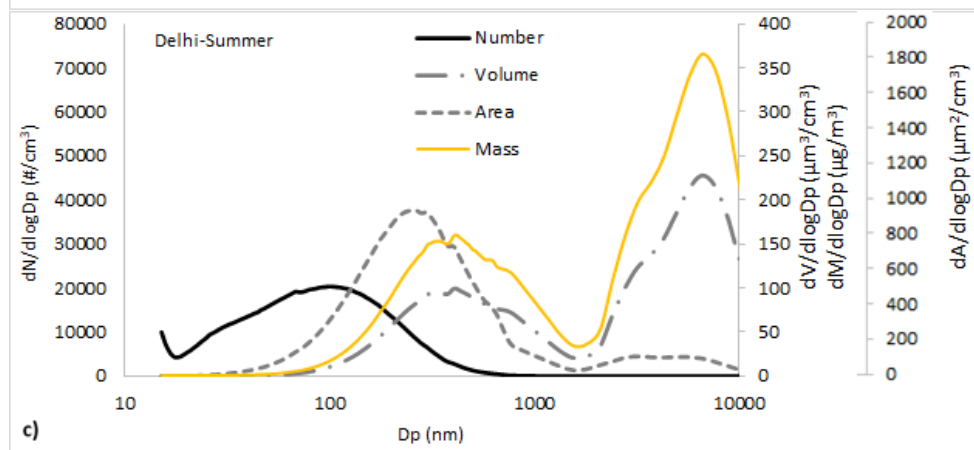
1027



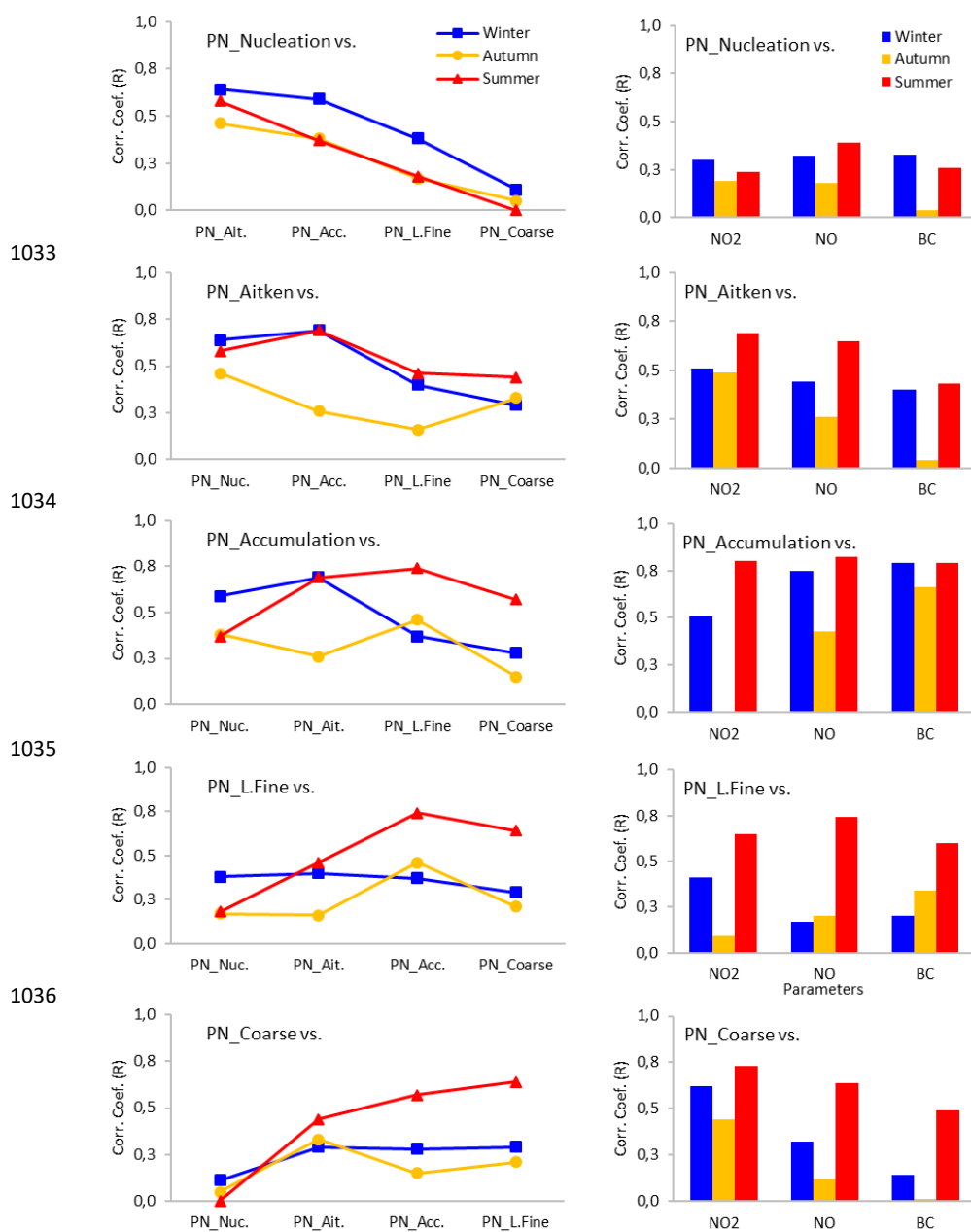
1028



1029



1030 **Figure 9.** Hourly average particle number, volume and area distributions in the winter (a), autumn  
1031 (b) and summer (c) in Delhi.  
1032



1033

1034

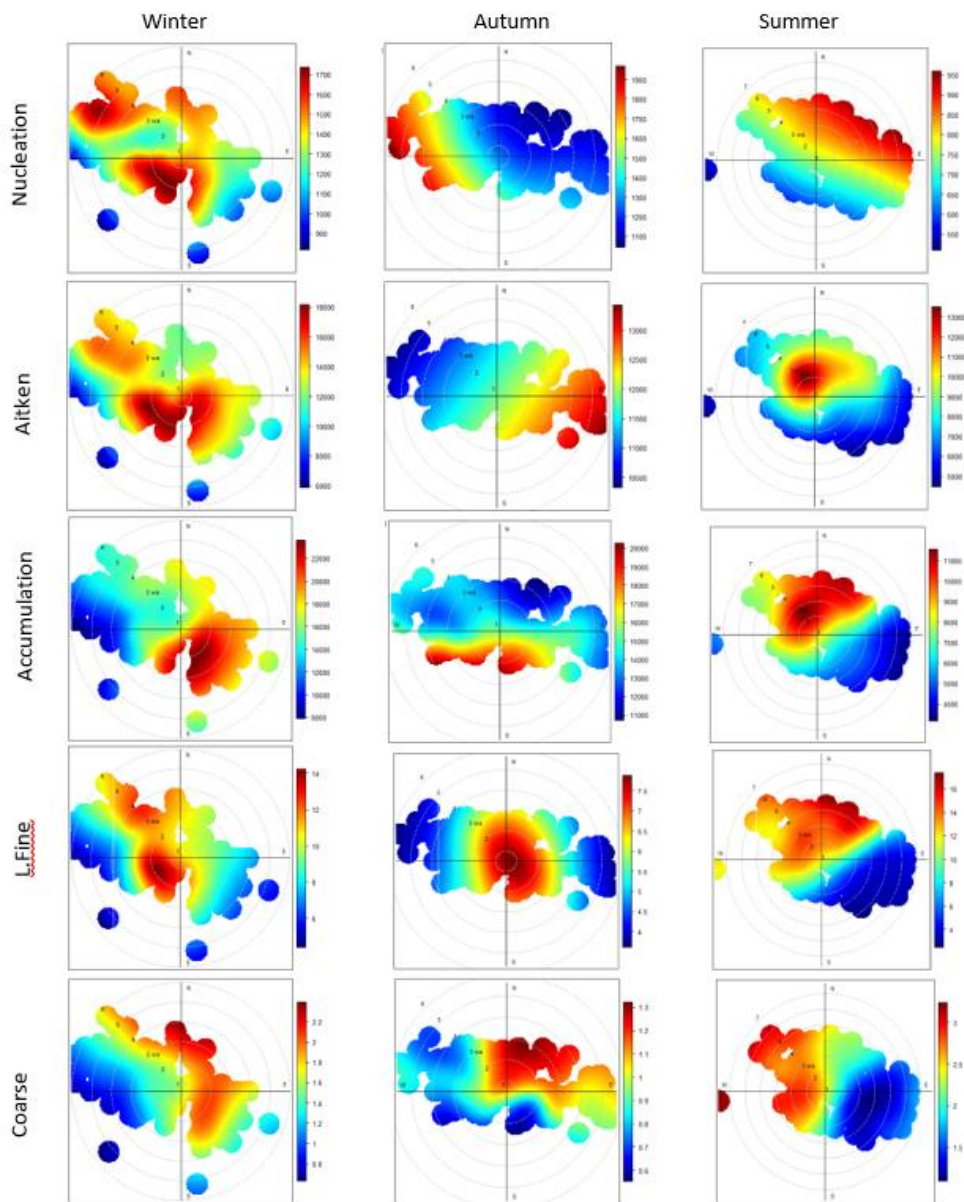
1035

1036

1037

1038

1039 **Figure 10.** Correlation coefficient (R) between the hourly average PNs of five particle size  
 1040 fractions (left side) and NO, NO<sub>2</sub>, BC (right side).  
 1041



1042

1043

1044 **Figure 11.** Polar plots of PNs ( $\#/cm^3$ ) for five particle size fractions in winter, autumn and summer  
1045 in Delhi.

1046